Subin et al., 2011

To be submitted to *JAMES*

An Improved Lake Model for Climate Simulations: Model Structure, Evaluation, and Sensitivity Analyses in CESM1

Zachary M. Subin [corresponding author]

Energy & Resources Group, University of California, Berkeley, and

Earth Sciences Division, Lawrence Berkeley National Laboratory

E-mail: zmsubin@lbl.gov

William J. Riley

Earth Sciences Division, Lawrence Berkeley National Laboratory

E-mail: wjriley@lbl.gov

Dmitrii Mironov

German Weather Service (DWD)

E-mail: Dmitrii.Mironov@dwd.de

Abstract

Lakes can influence regional climate, yet most general circulation models have simple and largely untested representations of lakes.

We developed the Lake, Ice, Snow, and Sediment Simulator (LISSS) for inclusion in the land-surface component (CLM4) of an earth system model (CESM1). The existing CLM4 lake model performed poorly at all sites tested; for temperate lakes, summer surface water temperature predictions were 10-25°C lower than observations. CLM4-LISSS modifies the existing model by including (1) a treatment of snow; (2) freezing, melting, and ice physics; (3) a sediment thermal submodel; (4) variable prescribed lake depth; (5) improved parameterizations of lake surface properties; (6) increased mixing under ice and in deep lakes; and (7) correction of previous errors. We evaluated the lake model predictions of water temperature and surface fluxes at three small temperate and boreal lakes where extensive observational data was available. We also evaluated the predicted water temperature and/or ice and snow thicknesses for ten other lakes where less comprehensive forcing observations were available. CLM4-LISSS performed very well compared to observations for shallow to medium-depth small lakes. For large, deep lakes, the under-prediction of mixing was improved by multiplying total thermal conductivity in lake liquid water by 10, consistent with previous published analyses. Surface temperature and surface flux predictions were improved when the aerodynamic roughness lengths were calculated as a function of friction velocity, rather than using a constant value of 1 mm or greater.

We evaluated the sensitivity of surface energy fluxes to modeled lake processes and parameters. Large changes in monthly-averaged surface fluxes (up to 30 W m^{-2}) were found when excluding snow insulation or phase change physics and when varying the opacity, depth, albedo of melting lake ice, and mixing strength across ranges commonly found in real lakes. Typical variation among model parameterization choices can therefore cause local surface flux changes much larger than expected changes in greenhouse forcing.

We conclude that CLM4-LISSS adequately simulates lake water temperature and surface energy fluxes and is suitable for inclusion in global climate studies.

1. Introduction

Lakes typically have different albedo, greater subsurface heat conductance and effective heat capacity, and much lower surface roughness than surrounding land area. These properties are important for accurate prediction of climate at the regional scale in regions with large lake area (Dutra et al. 2010; Krinner 2003; Lofgren 1997; Long et al. 2007; Rouse et al. 2005; Samuelsson et al. 2010), and are important in regional energy budgets (Jeffries et al. 1999). Several modeling studies (Bonan 1995; Dutra et al. 2010; Krinner 2003; Samuelsson et al. 2010) have found significant changes in regional temperature with prognostic 1-dimensional (1D) lake models integrated in climate models.

The impacts of lakes on regional climate vary with location and season. In general, unfrozen lakes tend to suppress diurnal temperature variation as compared to surrounding land (Samuelsson et al. 2010). Some temperate and high-latitude lakes tend to be cooler than surrounding land in the early summer, which, combined with their smaller surface roughness, tends to reduce heat fluxes to the atmosphere during this season (Dutra et al. 2010; Krinner 2003; Lofgren 1997; Rouse et al. 2008), though in some locations decreases in albedo and cloudiness compensate for this reduction (Samuelsson et al. 2010). At sufficiently high surface temperatures typical of low latitudes, lakes can increase latent heat fluxes relative to surrounding land in all seasons (Dutra et al. 2010). Temperate and high-latitude lakes tend to be warmer than surrounding land in autumn, resulting in increased surface heat fluxes (Dutra et al. 2010; Lofgren 1997; Long et al. 2007; Rouse et al. 2008; Samuelsson et al. 2010). Autumn and early winter overturning and freezing lakes warm and moisten the boundary layer (Jeffries et al. 1999) until substantial snow insulation is present (Dutra et al. 2010), and can cause lake-effect precipitation downwind (Bates et al. 1993; Goyette et al. 2000; Kristovich and Braham 1998; Laird et al. 2009; Lofgren 2004; Samuelsson and Tjernstrom 2001). In contrast, melting lakes cool the boundary layer (Samuelsson et al. 2010) as compared to adjacent land.

Lake area, lake physical properties, and lake biogeochemistry may interact with climate change and other anthropogenic forcings. Climate warming can alter lake mixing regimes (Fang and Stefan 2009; King et al. 1997; Kirillin 2010; MacKay et al. 2009; McCormick and Fahnenstiel 1999; Perroud and Goyette 2010; Verburg and Hecky 2009) and ice cover duration

(Blenckner et al. 2002; Brown and Duguay 2010; Fang and Stefan 2009; Mueller et al. 2009; Saloranta et al. 2009; Vavrus et al. 1996; Vincent et al. 2008; Zhang and Jeffries 2000), which can cause feedbacks to regional climate change. Changes in temperature, mixing regimes (Peeters et al. 2007; Verburg and Hecky 2009), watershed hydrology (Kosten et al. 2009), and anthropogenic nutrient deposition in the watershed may alter lake biology (MacKay et al. 2009), which is a primary determinant of lake optical properties (Cristofor et al. 1994), itself a strong control over lake mixing regime (Cristofor et al. 1994; Hocking and Straskraba 1999; Houser 2006; Mazumder and Taylor 1994; Mazumder et al. 1990; Persson and Jones 2008). Changes in the balance of precipitation and evaporation in lake watersheds (Schindler 2009; Small et al. 2001) and anthropogenic diversion of source rivers (Small et al. 2001) may change lake depth or area. Climate warming may interact with thermokarst lake dynamics at high latitudes (Smith et al. 2005). Lakes may be significant components of the global carbon cycle (Duarte et al. 2008; Tranvik et al. 2009; Walter et al. 2007), so alterations in their biochemistry under climate change could be important (Cardille et al. 2009; Walter et al. 2006).

Current numerical weather prediction (NWP) models, regional climate models (RCMs), and global climate models (GCMs) typically have a highly simplified, and often untested, treatment of lakes. The Weather Research and Forecasting Model 3 (WRF3) (Skamarock et al. 2008) and versions of the HTESSEL land-surface scheme prior to recent model development (Dutra et al. 2010) prescribe temperatures of large lakes using sea surface temperature interpolation and ignore subgrid-scale lakes. Simple fixed mixed-layer or heat penetration models have been used in previous studies with the Canadian Regional Climate Model (Goyette et al. 2000; Plummer et al. 2006), Geophysical Fluid Dynamics Laboratory GCM (Lofgren 1997), RAMS (Lofgren 2004), and ECHAM (Hagemann et al. 2006). Some models with more sophisticated treatment of lakes ignore lake water freezing [e.g., Bonan (1995)] or snow insulation [e.g., Samuelsson et al. (2010)]. Most coupled land-surface/atmosphere models use datasets that under-estimate global lake area (Downing et al. 2006) and treat lakes as having constant depth and optical properties. However, lake depth (Rouse et al. 2005), optical properties (Hocking and Straskraba 1999), sediment (Fang and Stefan 1998; Golosov and Kirillin 2010), freezing (Brown and Duguay 2010), and snow insulation (Brown and Duguay 2010; Dutra et al. 2010) are important for accurately modeling lakes and their interactions with the atmosphere.

Efforts are underway to develop, refine, and integrate lake models into NWP models, RCMs, and GCMs (MacKay et al. 2009; Mironov et al. 2010a); to develop global datasets required to run these models (Kourzeneva 2010); and to compare the performance of these models across lakes of different geometries, optical properties, and climates (Martynov et al. 2010; Perroud et al. 2009; Stepanenko et al. 2010). Several different types of one-dimensional (1D) lake models have been developed [reviewed in Martynov et al. (2010), Perroud et al. (2009), and Stepanenko et al. (2010)]: (1) relatively simple 2-layer models based on similarity theory [e.g., FLake (Mironov et al. 2010b)]; (2) thermal diffusion models with parameterized eddy diffusivity [e.g., the Hostetler Model (Hostetler and Bartlein 1990) and Minlake (Fang and Stefan 1996)]; (3) and more complex turbulence models [e.g., the Lagrangian model DYRESM (Yeates and Imberger 2003) and the k-ε turbulence closure models SIMSTRAT (Goudsmit et al. 2002) and LAKE (Stepanenko and Lykossov 2005; Stepanenko et al. 2011)].

Each of these 1D lake model types has advantages and disadvantages (Martynov et al. 2010; Perroud et al. 2009; Stepanenko et al. 2010). FLake is computationally efficient and performs reasonably across lake categories in predicting surface temperatures and ice characteristics. However, seasonal stratification is not always predicted well, and the model's two-layer structure causes difficulties simulating the water temperature near the bottom of deep lakes. The Hostetler Model predicts Sparkling Lake water temperatures well (Martynov et al. 2010; Stepanenko et al. 2010) but under-predicts mixing for several deep lakes (Martynov et al. 2010; Perroud et al. 2009; Stepanenko et al. 2010). Turbulence models improve characterization of Lake Geneva and Lake Michigan (Perroud et al. 2009; Stepanenko et al. 2010) by including additional sources of turbulence such as seiches (lake-scale wave motions), but over-predict mixing in Sparkling Lake (Stepanenko et al. 2010). Turbulence models can be computationally expensive, may require extensive lake-specific data or calibration, and have not yet been integrated into climate models.

In this study, we focused on the treatment of lakes in CLM4 (Community Land Model 4) (Lawrence et al. 2011; Oleson et al. 2010), the land component of the Community Earth System Model 1 (CESM1, http://www.cesm.ucar.edu/models/cesm1.0/) (Gent et al. 2011). The existing CLM4 lake model is identical to the version in CLM2 (Bonan et al. 2002b; Zeng et al. 2002), is based on Hostetler and Bartlein (1990), and incorporates code from LSM (Bonan 1995) and CoLM (Dai et al. 2003), but it has not been compared to observations in its current form. We

created CLM4-LISSS (Lake, Ice, Snow, and Sediment Simulator) by (1) including a comprehensive treatment of snow; (2) including freezing and melting (hereafter referred to as "phase change") and ice physics; (3) including a sediment thermal submodel; (4) allowing for variable prescribed lake depth; (5) improving the parameterization of lake surface properties such as roughness lengths; (6) increasing mixing under ice and in deep lakes, and (7) correcting several errors in the calculation of surface fluxes and lake temperature. We evaluated CLM4-LISSS at thirteen lakes and performed sensitivity experiments in order to characterize the effect of dominant processes and poorly constrained parameters on lake water temperature and surface energy flux predictions.

2. Methods

2.1 Model Description

2.1.1 Overview

CLM4-LISSS solves the 1D thermal diffusion equation by dividing the sub-surface into several discrete layers corresponding to: snow (when snow is present and greater than a minimum thickness); lake liquid water and ice (referred to collectively as the "lake body"); and underlying substrates (sediment, soil, and bedrock; hereafter referred to collectively as "sediment" except where otherwise noted). Sensible heat, latent heat, momentum, and radiation fluxes are calculated between the surface and the lower atmosphere (i.e., an observation height or atmospheric model bottom level, ~2 – 60 m). The residual energy flux at the surface is then used as a top boundary condition for thermal diffusion in the snow, lake body, and sediment. Constant lake body water content and saturated sediments are assumed, although the snow depth and properties are prognosed (Sec. 2.1.3). CLM4 uses a subgrid "tile" approach in which several landunit types are modeled separately (without explicit subgrid location or distribution) and the surface fluxes are averaged to the gridcell weighted by landunit area (Bonan et al. 2002a; Oleson et al. 2010), so lakes need not be resolved at the grid scale in order to be included. (The CLM software includes a four-level hierarchy containing gridcells, landunits, columns, and plant functional types. There are five distinct 1D landunits which do not exchange horizontal fluxes: soil, urban, lake, wetland, and glacier.) Currently, only one lake is modeled in each gridcell, but

the CLM4 software allows the flexibility for multiple lakes (e.g., of different geometry or optical categories) to be modeled in each gridcell (as multiple columns in the lake landunit).

In the lake body, mixing is caused by wind-driven eddies (Hostetler and Bartlein 1990), convection (Hostetler and Bartlein 1990), molecular diffusion, and unresolved 3D mixing processes (Fang and Stefan 1996). Shortwave [i.e., solar visible and near-infrared (NIR)] radiation is distributed among the snow and lake body according to their diagnosed optical properties. The submodels for friction velocity, aerodynamic resistances, snow, and sediment are similar to those in CLM4 (Oleson et al. 2010). The lake model is summarized in Fig. 1 and described in the following subsections; more details are included in the technical note available in the Supplementary (Supp.) Information. The CLM4-LISSS model also includes a correction of several structural deficiencies and errors in formulation in the existing CLM4 lake model (Appendix, Sec. 7.1).

2.1.2 Phase Change and Ice in the Lake Body

The lake body consists of a number of combined liquid water and ice layers; 25 layers are currently used for site evaluations, while 10 layers are currently used for global simulations in order to reduce computational expense. Each of these layers has a fixed water mass and fixed nominal thickness Δz (m), while the ice fraction (f_i) may vary from 0 to 1. The ice thermal conductivity is decreased by the ratio of ice density to water density to account for the increased physical thickness of the ice relative to the same mass of water. The heat capacity of each layer is the sum of the heat capacity of the ice mass and liquid water mass. The net thermal conductance κ (m s^{-1}) of layers containing both liquid water and ice is calculated by adding the respective resistances r (s m^{-1}) in series, assuming that the ice is stacked vertically on the liquid water:

$$\kappa = \left(r_w + r_i\right)^{-1} = \frac{1}{\Delta z}\left(\frac{1-f_i}{d_w} + \frac{f_i}{d_i}\right)^{-1}, \qquad \textbf{Eq. 1}$$

where d_w (m^2 s^{-1}) is the liquid water diffusivity and d_i (m^2 s^{-1}) is the ice diffusivity reduced by the ratio of ice density to water density. Liquid water diffusivity includes wind-driven eddy diffusivity (when there is no ice above the liquid), molecular diffusivity, and enhanced diffusivity (Sec. 2.1.6); ice diffusivity contains only molecular diffusivity.

At each time step, diffusion is first calculated ignoring phase change, and then phase change is calculated as a correction. This procedure is similar to the phase change solution for soil water and ice in CLM4. After the diffusion equation is solved (2.1.9), any layer containing nonzero ice fraction at a temperature above freezing (or nonzero liquid fraction at a temperature below freezing) undergoes freezing (melting) until either the energy excess (deficit) is consumed, or all the ice (liquid) is melted (frozen). Heat capacities are adjusted to precisely conserve energy as the ice fraction changes. After this process is complete, every layer containing both liquid water and ice must have a temperature at the freezing point. [Except for sensitivity experiments, ice is immediately aggregated at the top of the lake (Sec. 2.1.6).] This approach is a flexible solution to the Stefan problem (diffusion in the presence of a phase boundary) that (1) allows for an arbitrary temperature profile to occur in the ice (within the precision of the resolved layer thicknesses); (2) allows complex layering of water and ice (e.g., slush); (3) precisely conserves energy; and (4) is computationally simple.

2.1.3 Snow

The lake snow model used here is nearly identical to the snow model used over non-lake landunits in CLM4 (Lawrence et al. 2011). Once the snow thickness exceeds a small threshold, one or more snow layers are explicitly resolved with state variables including temperature, water content, ice content, density, snow grain radius, and accumulated deposited aerosols of several species. The shortwave radiation absorption, reflection, and transmission of each snow layer are calculated as a function of the snow grain radius and aerosol content (Flanner and Zender 2006; Flanner et al. 2007). Top snow layers can undergo evaporation, sublimation, and deposition of dew and frost. All snow layers can partially melt, refreeze, and allow infiltration of water into snow layers below. Currently, the model has up to 5 resolved snow layers, with explicit rules for subdividing thick snow layers and combining thin snow layers. Because a temperature gradient may occur between the top snow layer and the top lake layer, and the snow conductivity [based on the 1991 version of SNTHERM (Jin et al. 1999; Oleson et al. 2010)] considers air, water, and ice content, snow insulation is modeled explicitly in the diffusion solution.

There are several differences between the snow model used here over lakes and the model used for non-lake landunits in CLM4. For simplicity, freezing point depression is not allowed,

and the phase change solution is analogous to the solution used for lake layers (Sec. 2.1.2), except that layer ice and liquid water masses are the state variables rather than lake layer ice mass fraction. Snow is only allowed to begin to accumulate over lakes with a top layer containing nonzero ice fraction. If snow layers are found over a lake whose top layer is unfrozen, and the heat content of the top layer is enough to melt all the snow without completely freezing, then the snow is melted with heat from the top layer and eliminated.

When the snow is less than 40 mm thick, it does not form a resolved layer, and the only state variables are the ice mass and snow thickness. When the top lake layer is above freezing after the thermal transport solution with less than 40 mm of snow, the excess heat content (above freezing) is used to melt the snow. For non-lake landunits in CLM4, the minimum resolved snow layer thickness is 10 mm. However, during testing, we found occasional numerical instability when the Courant-Friedrich-Lewy condition (Hazewinkel 1995) was violated in the top snow layer; although the semi-implicit Crank-Nicholson method (Sec. 2.1.9) should be stable even when this condition is violated, the surface flux solution method (Sec. 2.1.8) acts as a fully explicit time-stepping component in the integration method and may compromise stability. We resolved this problem by requiring resolved snow layers to be at least 40 mm thick over lakes for the default 30 min model timestep, with appropriate adjustment to the rules for subdividing and combining snow layers. This type of instability has not been observed in non-lake landunits in CLM4, where the surface flux solution method differs somewhat (Sec. 2.1.8).

2.1.4 Sediment, Soil, and Bedrock

The new lake sediment model is similar to the soil and bedrock model for the CLM4 soil landunit. Soil physical properties, including the pore volume, heat capacity, and thermal conductivity are set as in CLM4 (Farouki 1981; Lawrence et al. 2008; Oleson et al. 2010), based on the prescribed soil texture and organic matter content in addition to the time-varying water and ice contents. The treatment of organic matter interpolates between pure mineral soil and pure peat properties as the organic matter fraction increases (Lawrence and Slater 2008). Dry, hydrologically inactive bedrock layers are found beneath the soil layers, with thermal conductivity [Clauser and Huenges in Ahrens (1995)] and heat capacity (Farouki 1981) set as in CLM4.

Subin et al., 2011

The primary difference between the treatment of soil in the CLM4 soil landunit and in CLM4-LISSS is that the sediment layers beneath the lake are maintained at hydraulic saturation. In addition, the thermal conductivity is adjusted during freezing to account for frost heave (e.g., a slight physical expansion in the layer due to the freezing of the saturated pore space, which for computational simplicity is treated by altering the thermal conductivity rather than the layer thickness), allowing excess ground ice in permafrost regions to be readily modeled in future experiments. We note that frost heave is ignored in the CLM4 soil landunit. Finally, freezing point depression is not allowed under lakes, as the freezing point depression in the CLM4 soil landunit is intended primarily to smoothly modulate the hydraulic conductivity and microbial activity just below freezing (Lawrence et al. 2011). The phase change solution for lake sediment is conceptually identical to the solution for phase change in lake water (Sec. 2.1.2) and snow (Sec. 2.1.3).

Currently, 3.8 m of sediment layers under lakes are included and initialized using the same global geographic soil texture and organic content data as for the soil landunit in CLM4 (Lawrence et al. 2008), with 38 m of bedrock below. This approximation may be reasonable for thermokarst and other transient or shallow lakes, but it is likely to be less accurate for deep lakes. However, deep lakes will be relatively insensitive to the thermal properties of the sediment, so this approximation should suffice until geographic data on sediment properties are available.

2.1.5 Radiation Transfer in Lake Body

For unfrozen lakes, radiation transfer is calculated similarly to Bonan (1995), with a fraction of the non-reflecting shortwave radiation absorbed near the lake surface (top 0.6 m), and the remainder absorbed in the lake according to the Beer-Lambert Law with a constant extinction coefficient. However, the fraction of non-reflected shortwave radiation absorbed at the surface, β, is set equal to the NIR fraction (> 700 nm) predicted by the atmospheric model or forcing data, which is typically ~0.5. When only the total shortwave radiation is provided as forcing data, CESM1 calculates a diagnostic NIR fraction. Any shortwave radiation penetrating the bottom layer of the lake body is assumed to be absorbed in the top layer of sediment, which is a good approximation except for an especially shallow and clear lake, where some radiation might be

reflected by the lake bottom and either absorbed in the layers above or released to the atmosphere, increasing the lake albedo.

The extinction coefficient, η (m^{-1}), is allowed to vary between gridcells. If not provided to the model as external data, η is calculated as a simple empirical function of lake depth, based on data from 88 Swedish lakes (Hakanson 1995) [using the Poole-Atkins expression (Idso and Gilbert 1974) to substitute η for the regressed Secchi Depth]:

$$\eta = 1.1925\, d^{-0.424}, \qquad \textbf{Eq. 2}$$

where d is the lake depth (m). For the lakes simulated in this study, the observed η varied between 0.05 and 7.1 m^{-1}. This parameter cannot be consistently calculated from physical properties of the lake or its climate, as it depends on lake biology that itself depends on nutrient runoff from the watershed (Cristofor et al. 1994). However, we hypothesize that shallow lakes may tend to have higher concentrations of suspended sediment and nutrients. Even though the regression to lake depth only explains 46% of the variance in Secchi Depth [Hakanson (1995), Table 4D], and the sample used in this regression may not be representative of lake optical variation globally, we contend that it is better to capture some of this variation than use a single global constant value, as lake optics are a strong control on lake mixing regime (Cristofor et al. 1994; Hocking and Straskraba 1999; Houser 2006; Mazumder and Taylor 1994; Mazumder et al. 1990; Persson and Jones 2008). Eq. 2 will introduce error for deep, turbid lakes, and we analyze the model sensitivity to opacity in Sec 3.2.4.

For frozen lakes with snow less than 40 mm deep, CLM4-LISSS assumes that the surface absorption (β) equals the NIR fraction of incident shortwave, and the remainder of non-reflected shortwave radiation is absorbed in the top lake body layer. For lakes with resolved snow layers (i.e., deeper than 40 mm), CLM4 contains a snow-optics and radiation transfer submodel that predicts snow layer optical characteristics, including transmissivity, based on predicted snow-grain radius and deposited aerosol species (Flanner and Zender 2006; Flanner et al. 2007). In this case, the CLM4 snow-optics submodel predictions are used in assigning absorbed shortwave radiation to snow layers. Because CLM4-LISSS, unlike non-lake CLM4 landunits, includes an infinitesimal surface interface used for calculating surface fluxes, we set β to be the fraction of shortwave radiation predicted to be absorbed by the top layer in the CLM4 snow-optics

submodel. For this model version, we assumed that any shortwave radiation penetrating the snow is absorbed in the top layer of lake ice, although some studies have suggested that radiation penetrating ice in the spring may induce convection (Mironov et al. 2002); future model versions should investigate this mechanism.

2.1.6 Mixing in the Lake Body

There are four types of mixing among layers of the lake water and ice: wind-driven eddy diffusion, buoyant convection, molecular diffusion, and additional background mixing due to unresolved processes (referred to as “enhanced diffusion”). In lake liquid water, CLM4-LISSS assumes the wind-driven eddy diffusivity, molecular diffusivity, and enhanced diffusivity are added independently; this approach differs little in practice from using the maximum over these different diffusivities, as they tend to vary by at least an order of magnitude (when present). For lake ice, only the molecular diffusivity is used. For model layers containing both water and ice, the ice is assumed to be stacked vertically on top of the water, so that the respective thermal resistances add in series to yield the total resistance of the layer (Eq. 1).

Wind-driven eddy diffusivity for unfrozen lakes is evaluated at each depth as a function of the 2 m windspeed, the Brunt-Väisälä frequency implied by the lake density gradient, and the latitudinally-dependent Ekman decay (Hostetler and Bartlein 1990). Although the friction velocity might be a better predictor than the 2 m windspeed, we chose to keep this portion of the Hostetler Model formulation unchanged. Wind-driven mixing tends to be stronger at higher wind speeds and for weakly stable stratification of the lake water, and it tends to penetrate deeper into lakes at low latitude.

Enhanced diffusion in lake water is intended to partially account for sources of turbulence other than wind-driven eddies that lead to mixing in frozen lakes and below the depth where wind-driven mixing can penetrate, including lake-scale wave motions like seiches and advection due to horizontal temperature gradients in large lakes. The Hostetler lake model, mixed primarily by wind-driven eddies, tends to under-predict mixing for frozen and deep lakes (Martynov et al. 2010; Perroud et al. 2009; Stepanenko et al. 2010), leading to insufficient heat loss for deep lakes in the winter, excessively fast warm-up in the spring (Martynov et al. 2010), and insufficient seasonal variation in lake bottom temperature (Perroud et al. 2009). Fang and Stefan (1996)

reasoned that in real lakes there will generally be some source of turbulence in addition to eddies created by wind at the surface, even below ice or at large depth. Turbulent kinetic energy tends to be reduced as a function of the Brunt-Väisälä frequency: under stably stratified conditions, the greater the density gradient, the faster turbulent kinetic energy will be dissipated, leading to a smaller effective diffusivity. Fang and Stefan (1996) suggest using the following expression for thermal diffusivity, K_{ed} ($m^2\ s^{-1}$), derived from measurements under an ice-covered lake (Ellis et al. 1991):

$$K_{ed} = 1.04\times10^{-8}\left(n^2\right)^{-0.43}, \qquad \textbf{Eq. 3}$$

where n (s^{-1}) is the Brunt-Väisälä frequency. For the calculation of K_{ed}, n^2 is limited to a minimum value of $7.5\times10^{-5}\,s^{-2}$ (Fang and Stefan 1996; Hondzo and Stefan 1993), which leads to a maximum K_{ed} of about 6 times larger than the molecular thermal diffusivity of water. For comparison, wind-driven eddy diffusivities calculated according to Hostetler and Bartlein (1990) are typically 2 to 3 orders of magnitude larger than the molecular diffusivity. Consequently, enhanced diffusion tends to only be important for frozen or deep lakes. We incorporated enhanced diffusion while noting that this is a somewhat ad hoc formulation and is not intended to fully compensate for missing 3D mixing processes: much stronger mixing (equivalent to a factor of ~10^3 increase in diffusivity) may sometimes be required to provide satisfactory simulations of deep lakes like Lake Michigan (Martynov et al. 2010). As such large values may occur unpredictably given the information available for a GCM and are likely to degrade the simulation of shallow lakes, we avoid using them in the baseline model configuration. We do, however, perform sensitivity experiments when evaluating model performance at deep lakes by increasing enhanced and eddy diffusivities by a factor of 10^1 – 10^2.

The lake density is recalculated after surface fluxes, radiation, diffusion, and phase change are calculated. If there is an unstable density profile between any two model layers j and j + 1, fast convection is assumed to occur that leaves the lake completely well-mixed (i.e., constant temperature, except in the presence of ice, as described below) from the top down through layer j + 1 (Hostetler and Bartlein 1990). This convective adjustment procedure is repeated iteratively, starting with the top two layers and proceeding downwards to the bottom of the lake, so that the density profile becomes stable or neutral. Except for sensitivity studies, the model assumes that

all of the ice will be located at the top of the lake. Consequently, convection is triggered any time ice occurs below water after phase change has been calculated. The model conserves total heat content and ice mass during this convection. If the total prior heat content of the layers undergoing convection is greater than that required to bring them to freezing, then the excess heat is assigned uniformly to the layers that are fully unfrozen after convection; otherwise, the heat deficit is assigned uniformly to the layers that are completely frozen after convection.

2.1.7 Surface Properties and Parameters

The albedo a for direct shortwave radiation striking unfrozen lakes is based on the form in Pivovarov (1972), with coefficients incorporated into CLM from BATS (Zeng et al. 2002) (Yongjiu Dai, personal communication, 2010):

$$a = \frac{0.05}{\cos z + 0.15}, \qquad \textbf{Eq. 4}$$

where z is the zenith angle. As the diffuse radiation calculated by the atmosphere or diagnosed from the atmospheric forcing is integrated over all angles, the albedo for diffuse radiation is the integral of Eq. 4 over the full sky, or 0.10. For cold, frozen lakes with snow depth < 40 mm, the albedo is set to 0.60 for visible radiation (< 700 nm) and 0.40 for NIR (> 700 nm), as in LSM (Bonan 1998; Bonan 1995). When snow is present, the albedo of the snow is calculated as in CLM4 for non-lake landunits (Flanner and Zender 2006; Flanner et al. 2007), and the overall albedo is the average of the snow albedo and ice albedo, weighted by the snow fraction (Lawrence et al. 2011). As real melting lakes can form puddles of liquid water above the ice or undergo disintegration of the ice surface, lowering the albedo and increasing the melt rate, we reduce the albedo for frozen lakes with snow depth < 40 mm whose top layer is close to freezing, following Mironov et al. (2010a):

$$a = a_0(1-x) + a_1 x, x = \exp\left(-95\frac{T_f - T_s}{T_f}\right), \qquad \textbf{Eq. 5}$$

where a_0 is the albedo for cold, frozen lakes with snow depth < 40 mm, T_f is the freezing temperature, a_1 = 0.10, and T_s is the surface ice temperature. We restrict a to be no smaller than that defined by Eq. 4.

Subin et al., 2011

The model assumes that lakes have a fixed emissivity of 0.97 (Oleson et al. 2010). The fraction of radiation absorbed near the surface of the lake (β) is described in Sec. 2.1.5.

The momentum roughness length (z_{0m}) for lakes with resolved snow layers is 2.4 mm as in CLM4 , with the scalar roughness lengths calculated as a function of the momentum roughness length and the friction velocity in the atmospheric surface layer (u_*), as in CLM4 over non-vegetated soil and snow (Zilitinkevich 1972):

$$R_0 = \frac{z_{0m} u_*}{\nu}, \qquad \textbf{Eq. 6}$$
$$z_{0h} = z_{0q} = z_{0m} \exp\left\{-0.13 R_0^{0.45}\right\}$$

where R_0 is the near-surface atmospheric roughness Reynolds number, z_{0h} is the roughness length for sensible heat, z_{0q} is the roughness length for latent heat, and ν is the kinematic viscosity of air.

In the absence of significant snow accumulation, z_{0m} is a crucial parameter for determining the friction velocity and thus the strength of the coupling between the lake and the atmosphere. We detail the treatment of unfrozen lakes below; for frozen lakes with snow depth < 40 mm, we apply z_{0m} = 1 mm, which is roughly consistent with literature values (Andreas 1987; Morris 1989; Vavrus et al. 1996). Scalar roughness lengths for frozen lakes with snow depth < 40 mm are calculated according to Eq. 6.

The roughness elements of unfrozen lakes are moving surface waves, whose development depends on the forcing wind, friction velocity, and fetch. The momentum transfer from the atmosphere to the lake depends on the size of the waves and the relative motion of the waves and the wind. Consequently, the effective z_{0m} is larger for lakes with small fetch, where the waves have not had a chance to equilibrate with the mean forcing wind (Donelan et al. 1993; Geernaert et al. 1987; Smith et al. 1992).

For the deep, open-water limit, z_{0m} is well-established (Atakturk and Katsaros 1999). In the limit of aerodynamically smooth flow and an established viscous sub-layer just above the lake surface (Fairall et al. 1996):

Subin et al., 2011

$$z_{0m} = \frac{\alpha \nu}{u_*}, \qquad \textbf{Eq. 7}$$

where α = 0.1 is a dimensionless empirical constant. In the limit of highly turbulent flow just above the surface:

$$z_{0m} = \frac{c u_*^{\ 2}}{g}, \qquad \textbf{Eq. 8}$$

where g is the acceleration of gravity and c is the dimensionless Charnock coefficient (Charnock 1955), equal to about 0.01 (Smith 1988). In CLM4-LISSS, we choose the appropriate limit by using the maximum of Eq. 7 and Eq. 8, which is equivalent to keeping R_0 no less than 0.1.

Under fetch-limited conditions, such as small lakes or lakes or oceans near the shoreline, the phase speed of the dominant wave mode is less than the forcing wind, and c is larger than the open water value (Donelan et al. 1993; Maat et al. 1991; Smith et al. 1992; Vickers and Mahrt 1997), though the precise value is not as well-characterized as the open water value. Moreover, small depth also limits the dominant phase speed (equal to $\sqrt{dg}$, where d is the depth, when the wavelength is much larger than the depth). Shoaling waves are steeper (Freilich and Guza 1984; Freilich et al. 1990) and so yield a larger c (Anctil and Donelan 1996; Vickers and Mahrt 1997), and it is typically asserted that small depth will increase the roughness length (Atakturk and Katsaros 1999; Smith et al. 1992). Panin et al. (2006) showed that without correcting for small depth, sensible and latent heat fluxes may be underestimated. However, we could not find systematic empirical relationships between c and d in the literature, and waves may be smaller for constant-depth shallow lakes than shoaling waves at the same depth near the shoreline of deep lakes. In addition, Gao et al. (2009) seemed to find smaller roughness lengths in a coastal zone as compared to open water, although they still observed larger roughness lengths for immature waves. Nevertheless, we tentatively included an increase in c for shallow lakes.

We based our formulation for c loosely on Vickers and Mahrt (1997), who found a mean value of c of 0.073 for offshore flow. The drag coefficient or roughness length is often expressed as a function of the dimensionless wave age, which is captured by the ratio u_*/c_p or u/c_p between the friction velocity or forcing wind and the dominant wave phase speed (Gao et al.

2009; Maat et al. 1991; Smith et al. 1992). In the absence of detailed wave information, this can be expressed as a power-law function of the dimensionless fetch (Mahrt 1999):

$$f = \left(Fg/u_*^{\,2}\right)^{1/3}, \qquad \textbf{Eq. 9}$$

where F is the fetch (m), and u is sometimes used instead of u_*. Vickers and Mahrt (1997) developed an expression for the drag coefficient that tends from the maximum fetch-limited value to the open-water value with $\exp\left\{-\frac{f}{f_c}\right\}$, where f_c = 100. We adjusted f_c to correspond to using u instead of u_* in Eq. 9, assuming a drag coefficient of 0.1, yielding f_c = 22. (As the drag coefficient varies over a large range, future model versions should eliminate this assumption by setting f_c = 100 and directly applying Eq. 9.) We used this relationship to calculate the fetch-limited c, and we also assumed that the depth limitation on c_p acts similarly to the fetch limitation in its effect on c:

$$\begin{aligned} c &= c_{\min} + (c_{\max} - c_{\min})\exp\{-\min(A,B)\} \\ A &= \left(\frac{Fg}{u^2}\right)^{1/3} \Big/ f_c \\ B &= \gamma\frac{\sqrt{dg}}{u} \end{aligned}, \qquad \textbf{Eq. 10}$$

where A and B define the fetch- and depth-limitation, respectively. We assumed $c_{\min}$ = 0.01 (the open-water limit) and $c_{\max}$ = 0.11, extrapolating roughly to the upper limit of the data in Vickers and Mahrt (1997). We tentatively set γ = 1, to be adjusted as data becomes available. For global simulations when the approximate fetch is unavailable, we may assume the fetch is 25 times the depth, a crude relationship characterizing typical lakes (Hutchinson 1957; Wetzel and Likens 1991). In this case, the depth limitation rarely takes precedence over the fetch limitation. This relationship will underestimate the fetch of broad, shallow lakes, but we reason that it is better to under-estimate the fetch than over-estimate it, as non-stationary wind will tend to keep the wave development farther from equilibrium. Alternatively, to reduce the number of unconstrained parameters causing differences between gridcells in global simulations, we can assume a fetch large enough that only the depth limitation on wave development applies. Either choice is crude

and should be replaced by global gridded data when available; we analyze the model sensitivity to fetch below.

For unfrozen lakes, the modeled scalar roughness lengths are separate functions of R_0 and z_{0m}, (Zilitinkevich et al. 2001):

$$z_{0h} = z_{0m} \exp\left\{-\frac{\kappa}{P_r}\left(4\sqrt{R_0} - 3.2\right)\right\},$$
$$z_{0q} = z_{0m} \exp\left\{-\frac{\kappa}{S_c}\left(4\sqrt{R_0} - 4.2\right)\right\}, \qquad \textbf{Eq. 11}$$

where κ is the von Karman constant, P_r = 0.71 is the molecular Prandt number for air, and S_c = 0.66 is the molecular Schmidt number for water in air. We arbitrarily imposed a lower limit of 0.01 mm on predicted scalar roughness lengths (coming into effect for u_* > ~0.2 m s^{-1}), as the Zilitinkevich et al. (2001) expressions have not been validated for very large u_*.

2.1.8 Surface Fluxes Solution

Surface fluxes are solved using the conditions at the atmospheric reference height as a top boundary condition and the top lake model layer temperature (in the lake body for snow depth < 40 mm and in the snow otherwise) as a bottom boundary condition, both evaluated at the end of the previous timestep. The surface temperature T_g is solved simultaneously with the friction velocity, surface roughnesses, and aerodynamic resistances in order to balance the surface energy budget. Note that T_g is associated with an infinitesimal interface between the top lake model layer and the atmosphere and thus can vary freely during the surface flux solution. This approach is in contrast with the surface flux solution over bare ground for non-lake landunits in CLM4, where the surface temperature is restricted to equal the top soil or snow layer temperature from the previous timestep (although the effective thickness is tuned to achieve appropriate diurnal temperature range), and thermal diffusion solution includes the first-order dependence of the surface temperature on the surface fluxes, which are then corrected after the diffusion solution.

Conservation of energy at the lake surface requires:

$$S + L = H + \lambda E + G, \qquad \textbf{Eq. 12}$$

where S is the absorbed shortwave radiation flux at the surface, L is the net longwave (thermal infrared) radiation flux at the surface, H is the downward sensible heat flux, λE is the downward latent heat flux, and G is the downward heat flux into the lake. These terms are calculated as:

$$
\begin{aligned}
S &= \beta S_a, \\
L &= -\varepsilon(\sigma T_g{}^4 - L_{atm}), \\
H &= \rho_{atm} c_p \frac{T_g - \theta_{atm}}{r_{ah}}, \\
\lambda E &= \lambda \rho_{atm} \frac{q_g - q_{atm}}{r_{aw}}, \\
G &= \lambda_T \frac{T_g - T_T}{\Delta z_T / 2},
\end{aligned}
\qquad \textbf{Eq. 13}
$$

where β is the fraction of the total surface absorbed shortwave radiation S_a (see 2.1.5), ε is the lake emissivity, σ is the Stefan-Boltzman constant, L_{atm} is the downward longwave radiation flux, ρ_{atm} is the moist atmospheric density, c_p is the specific heat of air at constant pressure, θ_{atm} is the potential temperature at the atmospheric reference height with respect to the surface (i.e., normalized to the reference height with an assumed lapse rate, not 1000 hPa), r_{ah} is the aerodynamic resistance with respect to sensible heat, λ is the latent heat of vaporization or sublimation (depending on the surface temperature), q_g is the saturated specific humidity at the surface temperature, q_{atm} is the specific humidity at the reference height, r_{aw} is the aerodynamic resistance with respect to latent heat, λ_T is the thermal conductivity of the top lake model layer, T_T is the temperature of the top lake model layer, and Δz_T is the top lake model layer thickness. For unfrozen lakes, λ_T includes eddy and enhanced diffusivities (2.1.6) in addition to molecular diffusivity, as calculated at the previous timestep.

The energy fluxes, aerodynamic resistances, and friction velocity all depend on the surface temperature. The friction velocity depends on the surface roughnesses, which in turn are functions of the friction velocity (Sec. 2.1.7). The system of equations is iterated four times to find the unique surface temperature T_g that balances the surface energy budget. During each iteration, the friction velocity and aerodynamic resistances are calculated according to the method for lakes or bare ground in CLM4, with the surface roughnesses calculated as in Sec. 2.1.7, using the values from the previous timestep for the first iteration. The updated

aerodynamic resistances are used to re-evaluate the surface fluxes, which are used to update the solution for surface temperature following the Newton-Raphson Method applied to Eq. 12.

After the surface temperature iteration yields a tentative solution T_g' for Eq. 12, several restrictions are imposed on T_g before the diffusion solution (Sec. 2.1.9) to maintain consistency with the top lake model layer temperature T_T:

$$\begin{aligned} &1)\, T_T \le T_f < T_g' \Rightarrow T_g = T_f, \\ &2)\, T_T > T_g' > T_m \Rightarrow T_g = T_T, \\ &3)\, T_m > T_g' > T_T > T_f \Rightarrow T_g = T_T. \end{aligned} \qquad \textbf{Eq. 14}$$

The first condition requires that, if there is any snow or ice present, the surface temperature is restricted to be less than or equal to freezing. The second and third conditions maintain convective stability in the top lake layer. For instance, if the surface temperature is less than the top lake layer temperature but greater than the maximum density temperature [T_m = 3.85°C as in Hostetler and Bartlein (1990), though we recommend 3.98°C for future model versions (Gebhart and Mollendorf 1977)], the water at the surface will be heavier than in the middle of the top layer, and mixing will immediately occur to homogenize the temperature in the top layer, so we reset the surface temperature to equal that of the top layer. This condition, which effectively extends the explicit convection to the top half of the top lake layer, is important for preventing unrealistic declines in lake surface temperature during night or during the autumn.

After T_g is potentially reset (Eq. 14), the longwave radiation and heat fluxes L, H, and λE are re-evaluated. Finally, G is set as the residual energy flux in Eq. 12, in order to precisely conserve energy: this may differ from the expression for G in Eq. 13 because of the restrictions imposed in Eq. 14 and the numerical precision of the iterative surface temperature solution. However, during model testing, the difference between the residual energy flux and the Eq. 13 expression for G in the absence of application of Eq. 14 was small (i.e., discrepancies at each timestep were generally less than 0.01 W m^{-2}, were always less than 2 W m^{-2}, and averaged to zero). Separate testing confirmed that the diagnostic calculation of surface roughness as a function of friction velocity, itself depending on surface roughness, did not adversely affect convergence of the T_g solution.

2.1.9 Diffusion Solution

After the surface fluxes, radiation transfer, and thermal conductivities are calculated, and before phase change, convection, and snow dynamics are evaluated (in that order), the 1D thermal diffusion equation is solved for the full lake column, including snow, ice, water, sediment, and bedrock:

$$c\frac{\partial T}{\partial t} = \frac{\partial}{\partial z}\left(k\frac{\partial T}{\partial z}\right) - \frac{d\phi}{dz}, \qquad \textbf{Eq. 15}$$

where c is the specific heat (per unit volume) at depth z (the sum of the respective heat capacities of the water, ice, and mineral constituents), T is the temperature, t is time, k is the thermal conductivity, and ϕ is the radiation flux reaching depth z. The top boundary condition prescribes the residual heat flux G calculated during the surface flux solution (2.1.8) to flow into the top layer, and the bottom boundary condition beneath the sediment prescribes zero heat flux to flow out of the bottom layer. Eq. 15 is discretized and solved using the semi-implicit Crank-Nicholson method; details are found in the technical note.

After diffusion, phase change, and convection are evaluated, an energy balance check is evaluated to make sure that the total change in lake enthalpy over the course of the timestep (including the latent heat associated with phase change and correcting for the discontinuity in specific heat at the freezing point) is equal to the shortwave radiation flux penetrating the lake surface $(1-\beta)S_a$ plus the heat flux transmitted from the lake surface G, to a precision of 10^{-7} W m^{-2}.

2.1.10 Hydrology

In CLM4-LISSS, the water content of melting snow is immediately added to runoff, as is done currently for glacier and wetland landunits in CLM4. Since the water level of the lake is fixed and watershed runoff into the lakes is not tracked, the water is balanced for global simulations by removing lake evaporation and sublimation from the runoff to the ocean, and adding dew, frost, and precipitation reaching the lake surface. Snow is accumulated for frozen lakes, and dew, frost, and precipitation are added to the top snow layer if present. Evaporation or sublimation may be removed directly from the top snow layer.

2.2 Model Evaluation

We evaluated CLM4-LISSS at two small temperate lakes (Sparkling Lake and Kossenblatter Lake) and one small boreal lake (Lake Valkea-Kotinen) where extensive observations were available, including lake water temperature, surface fluxes, optical extinction coefficient, and 2 m meteorological forcing observations above the lake including air temperature, humidity, pressure, and wind speed, with incoming longwave and shortwave radiation observations from nearby weather stations (Table 1). (We use “small lakes” to mean lakes smaller than ~2 km^2 in area, and “shallow lakes” to mean lakes with less than 20 m depth. “Large” and “deep” lakes mean the opposite.) We followed a similar evaluation procedure to that used in the Lake Model Intercomparison Project (LakeMIP) (Stepanenko et al. 2010) for Sparkling Lake, and CLM-LISSS is participating in the LakeMIP for Kossenblatter Lake and Lake Valkea-Kotinen. (Some of the results here will be compared to results from other models in Stepanenko et al., submitted to *Tellus A*.)

We also tested CLM4-LISSS at ten other lakes where complete meteorological forcing observations were unavailable and lake observation data were less comprehensive, including lakes spanning a large range of geometry, climate, and opacity (Table 1). Since most lake observations are limited to water temperature or water surface temperature and because snow and ice are key components of this lake model, we emphasized lakes where observations of snow and ice thickness were simultaneously made. Because we lacked meteorological forcing observations for any of these lakes, we sought several lakes in each category and for each observed variable of interest to compensate for the unpredictable discrepancies between coarse-scale meteorology and local conditions. Unfortunately, insufficient data were available to effectively evaluate the lake sediment temperature predictions. Finally, we evaluated the existing CLM4 lake model at four lakes for comparison: Sparkling Lake, Lake Michigan, Great Slave Lake, and Lake McIlwaine.

Each evaluation simulation was performed in single-point mode with a single lake column, using soil properties and aerosol deposition based on the nearest gridcell in the CLM4 1.9° x 2.5° dataset. For the large and deep lakes, we repeated the simulations with non-molecular thermal diffusivities multiplied by 10 in case the model (even with enhanced diffusion as in Sec. 2.1.6) insufficiently accounts for unresolved 3D processes; for Great Slave Lake we also performed a simulation with 100 times increased diffusivities.

In Sec. 3.1.1, we first analyze results from the three small temperate lakes where forcing observations were available, including testing the effects of the roughness length formulation. In Sec. 3.1.2, we examine ice and snow observations from Ryan Lake, Thrush Lake, Lake Gogebic, Big Island Lake, and Karujärv, with additional water temperature comparisons for boreal lakes Raksjo, Karujärv, and Thrush. We continue in Sec. 3.1.3 by considering Lake Michigan, a large, deep, temperate lake that undergoes mixing in excess of wind-driven eddies (Martynov et al. 2010), to characterize how the model fares under these conditions and to test the effects of enhanced diffusion and 10 times increased thermal conductivity. Great Slave Lake provides a similar test where some surface flux observations were also available. Finally, we briefly examine one very deep caldera lake (Crater Lake) and one mid-size tropical lake (McIlwaine).

2.3 Modeled Sensitivity of Surface Fluxes and Water Temperature to Processes and Parameters

Many lake models integrated in climate models lack some of the processes included in CLM4-LISSS, such as phase change and the insulation of frozen lakes by snow. There are also many lake characteristics and model parameters which are poorly constrained in global simulations and are sometimes characterized crudely in existing lake models, such as depth, surface roughness, and optical extinction coefficient. We performed sensitivity experiments to isolate the effects of each excluded process or typical range of parameter uncertainty on lake model predictions. We were primarily interested in the effects of these processes and parameters on global climate model predictions, so we examined the sensitivity of surface fluxes averaged over all the lake area in several regions, and examined changes in lake water temperatures for several representative gridcells to better understand the causes of flux changes. To understand the changes in surface fluxes, we also examined the rate of change of lake enthalpy, which we calculated as the sum of the rate of shortwave radiation absorption beneath the surface and the rate of heat diffusion into the lake at the surface (i.e., $(1-\beta)S_a + G$). For brevity, we analyzed averages for North Eurasian lakes only (e.g. 60 – 90°N, 0 – 175°E) in Sec. 3.2, using the simulated lake co-located with Finnish Lake Inari (“*Inarijärvi*”, 69.05°N, 27.81° E; simulated depth = 11 m) as a test case; figures for two warmer regions are available in the Supplemental (Supp.) Figures. In order to isolate the primary effects of processes and parameters without

atmospheric feedback, we used offline experiments forced by NCEP atmospheric reanalysis data (Qian et al. 2006).

We performed 14 total experiments, all independently varied from the reference case, detailed below. The reference case was a global 1.9° x 2.5° CLM4 simulation (with CLM4-LISSS) using year 2000 conditions for aerosol deposition and repeated 25-year periods of atmospheric forcing from 1980-2004, with 110 years for spinup and 15 years (1990-2004) for analysis. In order to make the reference simulation more realistic, we used lake depth and lake area data not available in the standard CLM4 surface datasets. The global lake area in the standard CLM4 dataset is about 0.7 million km^2, far less than the 2.7 million km^2 from the Global Lake and Wetland Database (GLWD) (Lehner and Doll 2004), which itself is probably an underestimate of the true lake area; Downing et al. (2006) estimated a total lake area of 4.6 million km^2. We used the GLWD lake area interpolated to 1.9° x 2.5° resolution and excluding the Caspian Sea (which is treated as ocean in CESM1), yielding 2.3 million km^2, shown in Supp. Fig. 1a.

To our knowledge, the first extensive global gridded lake depth dataset has been recently developed at 30 arcsec. resolution (Kourzeneva 2010) (http://www.flake.igb-berlin.de/ep-data.shtml). This dataset includes real data from a variety of sources for over 13,000 lakes and uses default depths of 10 m when a lake is present but the depth is not known, which is likely to be more realistic for the small lakes for which data are likely to be unavailable than the 50 m default lake depth in the existing CLM4. (Rivers are included in this dataset and assigned a depth of 3 m; even though the lake model may not be appropriate for rivers, we could not easily remove the rivers from the depth dataset, though these are not included in the GLWD that we used to determine the lake area simulated in each gridcell.) We interpolated this data to 1.9° x 2.5° resolution by using the mean depth from each 1 km gridcell in the lake-depth dataset where a lake was present, whether or not the real depth was available for that 1 km gridcell. Because the mean depth was used, each represented lake does not correspond to the depth of any particular real lake unless that lake dominates the 1.9° x 2.5° gridcell. This approximation is a crude first step intended to be more realistic than a constant global lake depth: future work should use multiple lake depth categories in each gridcell. Other interpolation approaches could have been used, such as using the mode rather than the mean lake depth when interpolating to the

coarse gridcell, or ignoring 1 km boxes assigned to the default 10 m in the lake depth dataset if at least one lake with known depth is available in the CLM4 gridcell; these alternative approaches are compared in Supp. Fig. 1b-d.

Each 25-year experiment started with the initial conditions after 100 years of spinup for the reference case and allowed 10 additional years for spinup (1980-1989 atmosphere) unless otherwise specified, using the final 15 years (1990-2004) for analysis, retaining year 2000 aerosol deposition. For simplicity, we assumed no small-fetch limitation on wave development (Sec. 2.1.7) in the reference case. The fourteen sensitivity experiments are described below. In addition to these fourteen experiments, we also investigated the effects of vertical discretization by comparing the model predictions when using 10 lake body layers for these global simulations as opposed to 25, which we used for the site evaluations.

1. *No heat of fusion for phase change*. We set the heat of fusion for water equal to 1 J kg^{-1}. All other effects of phase change (e.g., changes in albedo and thermal properties, suppression of wind-driven eddies) remained unchanged.
2. *No snow insulation*. We multiplied the thermal conductivity of snow by 10^6. All other snow properties remained unchanged.
3. *No enhanced diffusion.* The "enhanced diffusion" defined in Sec. 2.1.6 was turned off, leaving only the wind-driven eddy and molecular diffusion.
4. *Lake puddling*. We suppressed convection (which is normally responsible for aggregating ice at the surface) when more than 0.3 m of ice was present, allowing some liquid water to remain above ice and for arbitrary mixtures of ice and water to be present below. Wind-driven eddy diffusivity was added to liquid water present above ice. This case was compared to Case 11, as this mechanism independently allows a decrease in albedo when water is present over melting ice.
5. *Lake depth = 50 m.* All lakes had constant 50 m depth. Twenty years of additional spinup were used. This case was compared to a perturbed reference case with η = 0.22 m^{-1}, the default 50 m lake value (Sec. 2.1.5), so that the lake depth was the only change.

6. *Lake depth = 5 m.* All lakes had constant 5 m depth. This case was compared to a perturbed reference case with η = 0.60 m^{-1}, the default 5 m lake value (Sec. 2.1.5), so that the lake depth was the only change.
7. *η = 1.0 m^{-1}.* All lakes had constant extinction coefficient of 1.0 m^{-1}, instead of being a function of depth as in the reference case (Sec. 2.1.5). This represented an increase in extinction coefficient for most gridcells.
8. *z_{0m} = 1 mm.* All unfrozen lakes had constant roughness lengths (both momentum and scalar roughness lengths) equal to 1 mm, instead of the diagnostic values (Sec. 2.1.7).
9. *z_{0m} = 10 mm.* All unfrozen lakes had constant roughness lengths (both momentum and scalar roughness lengths) equal to 10 mm (the value used in the existing CLM4 lake model), instead of the diagnostic values (Sec. 2.1.7).
10. *Unfrozen albedo = 0.07.* All lakes had constant unfrozen albedo for both direct and diffuse shortwave radiation, instead of the relationships in Sec. 2.1.7.
11. *No albedo correction for melting lakes*. All frozen lakes had constant albedo (0.60 for visible and 0.40 for NIR), without reduction as the ice surface temperature approaches freezing (Sec. 2.1.7).
12. *Mixing times 2.* Wind-driven eddy and enhanced diffusion (Sec. 2.1.6) were multiplied by 2.
13. *Mixing times 10.* Wind-driven eddy and enhanced diffusion (Sec. 2.1.6) were multiplied by 10.
14. *100 m fetch.* The fetch was set to 100 m for all lakes, as opposed to the unlimited value in the reference case.

3. Results

3.1 Model Evaluation

3.1.1 Shallow Lakes with Forcing; Roughness Length Sensitivity

The existing CLM4 lake model performed poorly for Sparkling Lake (Fig. 2). During the summer, the lake was barely stratified and remained cold, with predicted surface water

temperature averaging 15°C too low. In the winter, the surface temperature sometimes rose well above freezing during warm spells, because of the model's lack of thermal inertia from the presence of ice. Latent heat fluxes were consistently high during the early summer and peaked too early in the season. Sensible heat fluxes were negative throughout the year. The model simulated an unrealistically high average diurnal surface temperature range exceeding 13°C during the summer, comparable to the average diurnal range in observed 2 m air temperature but not the average diurnal range in observed near-surface water temperature (0.5°C). Because the unphysical behavior of the existing CLM4 lake model at Sparkling Lake was evident at all other lakes tested, it served as a poor point of comparison for CLM4-LISSS, and we present further evaluation results only in the Appendix (Sec. 7.2).

CLM4-LISSS simulated medium-depth Sparkling Lake surface and 10 m water temperatures and sensible and latent heat fluxes well (Fig. 2). The latent heat flux predictions were higher than observations for 2002-2003 but accurate for 2004-2005, and the seasonal timing of the peak in latent heat flux was well reproduced. Sensible heat flux predictions were largely consistent with observations, though they peaked later in the season than observations. Predictions of summer diurnal temperature range were 0.8°C for the surface and 0.5°C for the water at 0.05 m, the latter being consistent with observations (not shown).

Degrading the roughness lengths from the diagnostic values (which ranged between 0.01 and 1 mm but were generally between 0.1 and 0.5 mm) to a constant 1 or 10 mm caused excessive latent heating and cold surface temperatures (Fig. 3). For 10 mm roughness lengths, summer latent heating was 46 W m^{-2} higher than when using the diagnostic roughness lengths, and near-surface summer water temperatures were 4.2°C too low compared to observations. This cold bias persisted into the winter, causing early freeze-up and late thaw dates.

The model evaluations at the two relatively shallow, turbid lakes (Kossenblatter and Valkea-Kotinen) showed similar results (Fig. 4 and Fig. 5). CLM4-LISSS simulated the Kossenblatter surface and 1 m temperatures relatively accurately, while using fixed 10 mm roughness lengths caused a cold bias. CLM4-LISSS mildly over-predicted Kossenblatter heat fluxes while reproducing the temporal patterns of variability; with fixed 10 mm roughness lengths latent heat fluxes were excessively high and sensible heat fluxes were excessively low. CLM4-LISSS

reproduced the observed vertical and seasonal patterns for water temperature and the seasonal patterns for afternoon heat fluxes for Lake Valkea-Kotinen [although these eddy covariance data are limited to conditions when the fetch is along the lake (Nordbo et al. 2011)].

3.1.2 Small Temperate and boreal Lakes: Ice, Snow, and Sediment

We evaluated simulated ice and snow thicknesses for Big Island Lake, Lake Gogebic, Ryan Lake, Thrush Lake, and Karujärv (Fig. 6 and Supp. Fig. 2). The model performed acceptably by correctly predicting the range of thickness magnitudes and the range of inter-annual variability among modeled years and between lakes. Freeze and thaw dates were approximately correct, given the sporadic available observations. As in the observations, the model showed a strong anti-correlation between snow and ice thicknesses, demonstrating that it correctly represented the inhibition of ice formation from snow insulation (Brown and Duguay 2010). However, predictions of snow thickness for a given year or lake were not consistently accurate. These differences were possibly influenced by inconsistencies between actual local snowfall and the snowfall predicted by the 2° reanalysis dataset.

We also evaluated water temperature predictions for temperate Thrush Lake (Supp. Fig. 3) and boreal lakes Raksjo (Supp. Fig. 4) and Karujärv (Supp. Fig. 2). The model predicted temperatures accurately for Thrush and Karujärv. The seasonal variation was mildly delayed and the heat penetration mildly under-predicted for Raksjo compared with observations, though the surface temperature variation was accurate.

3.1.3 Deep Lakes; Mixing Sensitivity

The parameterization of wind-driven eddy mixing (Hostetler and Bartlein 1990) apparently led to under-predicted mixing in all four simulated deep lakes, as slight improvement was obtained for some lakes with enhanced diffusion and substantial improvement was usually obtained for all four lakes when increasing thermal conductivity by 10 – 100. Even without these improvements, performance of CLM4-LISSS was adequate in the context of uncertain lake properties at the global scale (Sec. 3.2).

We evaluated Lake Michigan with CLM4-LISSS, CLM4-LISSS without enhanced diffusion, and CLM4-LISSS with 10 times increased thermal conductivity, compared to vertical water temperature observations (Fig. 7) and surface temperature observations (Fig. 8) for 1990. CLM4-

LISSS accurately predicted the observed seasonal and vertical patterns of variation in water temperature including summer stratification, although the predicted summer thermocline was too shallow (Fig. 7). Stratification was under-predicted with 10 times increased thermal conductivity.

Typical of the difficulties of evaluating 1D models for large lakes, surface temperature observations differed between the two mid-lake buoys closest to the simulated location by up to 5°C (Fig. 8). The warmer buoy had surface temperature observations colder than those of the nearby water temperature observations (Fig. 7) during the same time period. CLM4-LISSS predicted an earlier spring warm-up and slightly higher summer surface temperatures than the observations (Fig. 8). Including enhanced diffusion hastened the spring warm-up, inconsistent with observations, but had little effect during the summer and early autumn. When 10 times increased thermal conductivity was used, summer surface temperatures decreased to be within the range of the buoy observations, spring surface temperatures were closer to observations but still predicted to be up to 10°C too warm, and an early summer overturning event was much more pronounced than the observed. In the late autumn, using enhanced diffusion and especially 10 times increased thermal conductivity caused a delay in the freeze-up, consistent with observations.

We evaluated Great Slave Lake with CLM4-LISSS, CLM4-LISSS without enhanced diffusion, and CLM4-LISSS with 100 times increased thermal conductivity, compared to vertical water temperature observations and surface flux observations for 1997-2002 (Fig. 9). Compared to observations, CLM4-LISSS tended to under-predict mixing, as evidenced by over-predicted surface temperatures, under-predicted autumn 40 m water temperatures, an early peak in surface heat fluxes, and an early freeze-up date. These errors were most pronounced when enhanced diffusion was turned off, while substantial improvements were obtained with 100 times increased thermal conductivity. A comparison of each year's freeze-up and thaw dates between CLM4-LISSS simulations and observations (not shown), though complicated by the lack of fractional ice cover predictions, also suggested that the simulated seasonal dynamics were several weeks too early in the default version and about one week early with 100 times increased thermal conductivity. We note that errors in all simulations may have been exacerbated by the use of coarse resolution (~2°) reanalysis-derived meteorological forcing rather than local forcing, as air

temperatures over Great Slave Lake tend to have a substantial seasonal lag compared to air temperatures over nearby land (Rouse et al. 2008).

We also evaluated model predictions for the very deep (594 m) Crater Lake with mild Pacific Northwest climate and for tropical Lake McIlwaine. CLM4-LISSS reproduced the vertical and seasonal patterns of temperature variation in Crater Lake, which is well-mixed in the winter and mildly stratified in the summer, although it under-predicted seasonal temperature variability and summer stratification (Supp. Fig. 5 and 6). Predictions are closer to observations with 10 times increased thermal conductivity and farther from observations with no enhanced diffusion. CLM4-LISSS performed similarly for Lake McIlwaine, capturing the enhanced stratification and surface warming in the summer (Supp. Fig. 7). It over-predicted stratification in this case, but predictions were closer to observations with 10 times increased thermal conductivity and farther from observations with no enhanced diffusion.

3.2 Model Sensitivity

We evaluated the sensitivities to modeled processes and parameters for the average monthly surface energy fluxes for North Eurasian lakes and the water temperatures of the 11 m deep lake approximating Finnish Lake Inari. Summarizing the results detailed in the following subsections (3.2.1-3.2.7), we found very high sensitivity to the inclusion of snow insulation and high sensitivity to the inclusion of the heat of fusion for phase change, lake depth, extinction coefficient, and the albedo of melting lakes. Sensitivities to roughness lengths and mixing strength depended on the perturbation magnitudes. We found low sensitivities to enhanced diffusion (Case 3), the inclusion of puddling on thick melting ice (Case 4), the unfrozen albedo (Case 10), and the fetch (Case 14), so we do not discuss these cases below. Surface flux sensitivity and water temperature figures for all cases are available in the Supplemental Information (Supp. Fig. 10 – Supp. Fig. 18). Compared to the results detailed below, results from warmer regions (i.e., U.S. lakes and Eastern Hemisphere tropical lakes) showed reduced sensitivity to snow insulation and phase change and increased sensitivity to the roughness lengths, enhanced diffusion, and mixing strengths (Supp. Fig. 19 – 36).

3.2.1 Snow Insulation

In Case 2, we eliminated snow insulation by multiplying the thermal conductivity of snow by 10^6, keeping all other snow properties constant. North Eurasian lakes were predicted to lose ~20 W m^{-2} more to the atmosphere during the winter (Fig. 10a). Compared with the baseline simulation (Fig. 11a), Inari ice increased in thickness (~ 1 m) and duration (1 week) and cooled (~8°C) at the surface (Fig. 11b). North Eurasian lakes remained cooler in the summer, leading to an extra 30 W m^{-2} absorption in July, manifesting as large declines in summer longwave, latent, and sensible energy fluxes.

3.2.2 Heat of Fusion for Phase Change

In Case 1, we eliminated the heat of fusion of water. This modification dramatically increased the thickness of Inari winter lake "ice" and cooled its top layer by up to 4°C (Supp. Fig. 14b). The decline in North Eurasian lake surface temperatures caused less heat to be lost to the atmosphere during the winter, while faster spring melt decreased the lake energy uptake by 14 W m^{-2} in June, causing 2 – 3 W m^{-2} increases in longwave, latent, and sensible energy fluxes (Fig. 10b). It is noteworthy that both eliminating the heat of fusion and eliminating snow insulation caused declines in ice surface temperatures but with opposite effects on atmospheric fluxes and lake summer temperatures.

3.2.3 Lake Depth

In Case 5, we increased the depth of modeled North Eurasian lakes from an average of 14 m (with a median of 10 m) to a constant 50 m, while in Case 6, we decreased the depth to a constant 5 m. Decreasing the depth led to the expected summer warming and autumn cooling of the Inari surface due to decreased thermal inertia (Supp. Fig. 15d), associated with a decrease in energy uptake of North Eurasian lakes by 5 W m^{-2} in the summer and an increase in lake energy loss of 12 W m^{-2} in October (Fig. 10c). During the summer, sensible and latent fluxes increased while net longwave fluxes remained nearly unchanged, indicating that the warming occurred primarily during the day.

The seasonal pattern of surface flux change was more complicated when the depth was increased. In June, North Eurasian lakes lost an extra 10 W m^{-2} to the atmosphere, primarily via longwave radiation (Fig. 10d). This loss is consistent with the predicted greater winter and spring temperature stratification under the ice and consequent delay in overturning as compared to the

baseline simulation with identical constant η (not shown). This change may have been unrealistic if winter below-ice mixing was too weak (Martynov et al. 2010). In contrast, energy uptake by the lakes increased by 14 W m^{-2} in September when the depth was increased to 50 m, primarily via decreases in latent heat fluxes. The lakes then returned an extra 8 W m^{-2} to the atmosphere in November.

3.2.4 Extinction Coefficient

Increasing the optical extinction coefficient of North Eurasian lakes from an average of 0.46 m^{-1} to a constant 1.0 m^{-1} (Case 7) acted analogously (though more strongly, in this case) to a decrease in lake depth, increasing thermal stratification and decreasing the effective mixing depth of Lake Inari during the summer (Fig. 11c). North Eurasian lake energy uptake in July decreased by 17 W m^{-2}, primarily via increased latent heat flux associated with a daytime surface warming; lake energy loss in October decreased by 16 W m^{-2}, about equally via sensible, latent, and longwave fluxes (Fig. 12a).

3.2.5 Melting Lake Albedo

In Case 11, we maintained the albedo of melting ice at the winter value rather than allowing it to decline to 0.10 as the exposed ice surface reached the melting temperature. This change caused a median of 8 days delay in melt for North Eurasian lakes, though much larger delays were observed in some gridcells. Energy uptake by lakes decreased by 15 W m^{-2} and energy fluxes to the atmosphere decreased by 16 W m^{-2} in June (Fig. 12b), associated with a loss of 31 W m^{-2} in absorbed shortwave radiation (not shown). Lakes remained colder in July, taking up an extra 15 W m^{-2}.

3.2.6 Roughness Lengths

In Case 8, we fixed roughness lengths for unfrozen lakes to a constant value of 1 mm [instead of the diagnostic values (Sec. 2.1.6), which varied but were generally less than 0.5 mm], while in Case 9, we increased roughness lengths to 10 mm, which is unrealistically high but equal to the values used in the existing CLM4 lake model. Fixing the roughness lengths at 1 mm caused about a 15 W m^{-2} increase in the sum of summer sensible and latent heat fluxes for North Eurasian lakes, at the expense of lake energy uptake and longwave fluxes (Fig. 12c). The Lake Inari peak summer surface temperature declined by 2°C (Supp. Fig. 16c). Lakes remained colder

in the autumn, with lake energy loss decreasing by 9 W m^{-2}, primarily via decreased longwave fluxes. These effects were magnified when roughness lengths were fixed at 10 mm, with about a 20 W m^{-2} summer increase in the sum of latent and sensible heat fluxes for North Eurasian lakes, a 19 W m^{-2} decline in October lake energy loss (Supp. Fig. 12a), and a 4°C decline in peak Inari summer surface temperature (Supp. Fig. 16d). In both cases, decreased summer energy uptake by Lake Inari led to an annually colder lake, with ~ 1 week earlier freeze-up and later thaw (Supp. Fig. 16c-d).

3.2.7 Mixing Strength

In Case 12, we multiplied eddy and enhanced diffusivities by 2, and in Case 13 we multiplied each by 10. Results were modest for the factor of 2 increase in thermal conductivity, increasing the July energy uptake and October energy loss for North Eurasian lakes by about 4 W m^{-2} (Supp. Fig. 12d). For the factor of 10 increase, the increase in seasonal energy exchange was about 20 W m^{-2} (Fig. 12d); Lake Inari summer thermal stratification also decreased (Fig. 11d). Normally, a low sensitivity to a 100% parameter change would be considered as evidence of low uncertainty, but the results in Sec. 3.1.3 suggested that the uncertainty in mixing strength for large, deep lakes is very large, and a factor of 10 increase usually improved the realism of simulated water temperatures. Consequently, the 20 W m^{-2} increase in seasonal energy exchange associated with Case 13 may be realistic.

3.2.8 Discretization

We also compared the model predictions when using 10 lake body layers for these global simulations as opposed to 25, which we used for the site evaluations. We found that errors in surface energy flux predictions may result from using 10 layers instead of 25 layers, with annual-mean errors of a few W m^{-2}. Much larger errors may occur for short time periods when energy exchange between the lake body and atmosphere are large. We therefore recommend increasing the number of layers for global simulations when sufficient computational resources are available.

4. Discussion

4.1 Performance of CESM/CLM4 Lake Models

Due to the lack of phase change physics and snow insulation, unrealistically large roughness lengths, and errors in the calculation of surface fluxes, surface temperature, and eddy diffusivity, predictions of the existing CLM4 lake model poorly matched observations at all lakes tested (Sec. 3.1.1 and 7.2). For the three small, shallow temperate and boreal lakes with available meteorological forcing observations, CLM4-LISSS predictions for water temperature were excellent, and predictions for surface fluxes were good. We note that there are important uncertainties associated with eddy-covariance observations, particularly in the presence of land-surface heterogeneity (Foken 2008), which certainly applies to these small lakes. For other small shallow temperate and boreal lakes without forcing observations, water temperature predictions were good, with no systematic biases. CLM4-LISSS performance was adequate for large and deep lakes (Sec. 4.3), although we note that there are substantial horizontal variations in temperature which CLM4-LISSS cannot resolve. Insufficient data were available to conclusively test the performance of the ice, snow, and sediment schemes in CLM4-LISSS, although there appear to be no systematic biases in the ice and snow thickness predictions, and the model showed the right seasonal behavior and a realistic anti-correlation between snow depth and ice thickness (Brown and Duguay 2010). The new roughness length formulations for momentum, heat, and moisture fluxes were clearly superior to fixed values of 1 mm or greater, although insufficient data were available to test the relatively uncertain enhancement of surface exchange due to depth and fetch limitation on wave development. However, sensitivity to fetch limitation appeared to be very small compared to the other parametric uncertainties, with a maximum of 2 W m^{-2} effects on monthly surface fluxes for North Eurasian lakes when changing from an unlimited to a 100 m fetch. Evaluation of model predictions of snow, ice, and sediment would benefit from the greater availability of measurements of snow thickness, ice thickness, and sediment temperatures at the same location as above-lake meteorological observations, including incident snowfall.

4.2 Ice and Snow

The largest model sensitivity we found for North Eurasian lakes was the presence or absence of snow insulation, which caused greater than 30 W m^{-2} monthly average changes in lake energy exchanges in the winter and summer. Indeed, while the historical development of climate models has generally emphasized snow over land surfaces rather than over lake and sea ice, snow there

may have relatively larger importance (per unit area) because of the relatively larger sub-surface heat capacity and conductivity for water and ice in the absence of snow insulation. The inclusion of snow insulation may affect predictions of lake-climate interactions (Sec. 4.5).

We successfully introduced a new method for modeling ice in lakes, allowing each layer to have an independently variable ice fraction rather than separately modeling ice above water layers. This framework may allow for more realistic prediction of temperature gradients in ice and more flexible treatment of surface ice fractionation or slushy mixtures of ice and water. Using this framework, we tested the impact of suppressing convection and allowing mixtures of ice and water to occur when ice is greater than 0.3 m thick, and found relatively low impacts on regional surface energy exchanges.

Future work could improve the treatment of lake ice during periods of marginal ice cover. It may be possible to parameterize surface ice fractional cover, which can be important for large lakes (Goyette et al. 2000). Such an approach may be more robust than simply decreasing the albedo over melting ice to account for puddling and disintegration, by being able to predict the large observed albedo variability during melt. Our current implementation caused large changes in surface fluxes (16 W m^{-2}) compared to assuming a constant winter-time ice albedo, and may be an over-estimate of the albedo decrease, as it allows melting lakes to have an albedo as low as unfrozen lakes under some combinations of zenith angle and ice surface temperature. For small high-latitude lakes, recent work suggests that puddling over melting ice may be more typical for lakes that freeze to the bottom each winter (Arp et al. 2011); this information could be used in predicting albedo declines and suppression of convection in melting lakes.

4.3 Mixing in Small and Large Lakes

Previous studies have shown that lake models parameterizing thermal conductivity based on wind-driven eddies (Hostetler and Bartlein 1990) and molecular diffusivity alone under-predict mixing for large, deep lakes (Martynov et al. 2010; Perroud et al. 2009; Stepanenko et al. 2010). That behavior was confirmed for all four simulated deep lakes, except at one of three observation sites for Lake Michigan. In some cases, we found slight improvement when adding enhanced diffusivity under conditions of neutral stability to represent unresolved 3D mixing processes (Fang and Stefan 1996), but this change was insufficient to bring thermal conductivity to realistic

levels. For deep lakes, we nearly always obtained substantial improvements in lake water temperature and surface flux predictions when we increased thermal conductivity by 10, and in one case predictions were further improved when increasing by 100. This sensitivity is consistent with the large thermal diffusivities found by Martynov et al. (2010) to be required to substantially improve the simulation of Lake Michigan compared to surface temperature observations.

Some 1D lake models tend to assume greater mixing, including both simpler models like FLake and more sophisticated *k*-*ε* models like SIMSTRAT that predict the production, dissipation, and diffusion of turbulent kinetic energy. Consequently, these models can sometimes more accurately predict temperatures in large, deep lakes like Lake Michigan and Lake Geneva than does the Hostetler Model (Martynov et al. 2010; Perroud et al. 2009; Stepanenko et al. 2010). However, when these turbulence models are applied to small, shallow lakes (e.g., Sparkling Lake), they can sometimes over-predict mixing, causing temperature predictions to not match observations as well as simpler models (Stepanenko et al. 2010). This discrepancy may be because the additional sources of turbulent kinetic energy parameterized in these models may be serving as a proxy for advection induced in large lakes by horizontal temperature gradients not able to be represented in 1D models, or that these models parameterize insufficient dissipation of turbulent kinetic energy for small lakes.

Further research is needed to bridge the gap between large and small lakes in GCM-scale lake models. For global simulations with CLM4-LISSS described here, it may be advisable to increase thermal conductivity by a factor that depends on lake shape, and future research should systematically investigate the relationship between mixing strength and lake geometry. For now, we recommend increasing the thermal conductivity strength by 10 for lakes larger and deeper than some threshold (e.g., 5 km^2 and 30 m). Additional research should also be undertaken to couple *k*-*ε* models into climate models. Another approach would be to couple 3D models into climate models for large lakes where detailed bathymetry is available (Leon et al. 2007; Song et al. 2004).

In any case, surface flux changes resulting from 10 times increased thermal conductivity in our model were comparable in magnitude to those changes resulting from changes in modeled

lake depth. Given the challenges in interpolating from fine-scale variation in lake depth to a single or small number of lake depths at the GCM scale, under-prediction of mixing for large lakes may be relatively unimportant for global simulations except in the vicinity of very large lakes like the Great Lakes. Indeed, the majority of global lake area is occupied by much smaller lakes (Kourzeneva 2010; Lehner and Doll 2004) for which CLM4-LISSS performance is very good.

4.4 Uncertain Parameters for Global Simulations

We found moderate changes in surface fluxes when the modeled lake depths of North Eurasian lakes were varied across a typical range. Until recently, most global simulations assumed constant lake depth. Fine resolution global data on lake depth are becoming available (Kourzeneva 2010), although spatial coverage is far from complete. It may also be possible to invert for lake depth by comparing modeled surface temperature to remotely sensed surface temperature (Balsamo et al. 2010; Dutra et al. 2010). However, in our current implementation, as in many other GCMs, only one lake is modeled in each gridcell, so even allowing the lake depth to vary between gridcells is a crude representation of real lake depths since most lakes are much smaller than the grid scale. Different interpolation approaches could be used to aggregate observed lake depths at finer scales to calculate the single representative gridcell lake depth, but it is not clear what the optimum gridcell depth would be. The optimum lake depth may depend on the model structure and intended application. A more sophisticated approach would be that used in Samuelsson et al. (2010), where several lakes of different depth categories are explicitly modeled in each RCM gridcell. Further research is needed to identify how best to aggregate lakes into depth categories.

Increasing the extinction coefficient from an average of 0.46 m^{-1} to a constant 1.0 m^{-1} for North Eurasian lakes caused large changes in surface fluxes and differences between summer surface and lake bottom temperatures, despite being a relatively small change compared to the large variability of observed values (0.05 to 7.1 m^{-1} just for the lakes simulated in this study). Such increases in thermal stratification with increased opacity have been observed elsewhere and could affect lake-climate interactions (Sec. 4.5). The surface flux changes were similar in seasonal pattern but larger in magnitude than those resulting when decreasing the depth from a

median of 10 m to a constant 5 m. Consequently, global data on lake opacity may be as important as, or more important than, global data on lake depth. It may be possible to retrieve lake opacity from satellite observations (Gomez et al. 2009; Koponen et al. 2002; Zhang et al. 2003). However, without explicitly modeling several lakes of different optical categories in each gridcell, it is unclear what the optimum extinction coefficient should be for the single modeled lake in each gridcell, or whether such an optimum value would be model-dependent. Moreover, we assumed that the extinction coefficient is not related to albedo, but further work is needed to understand the relationship, if any, between lake opacity and albedo.

In contrast, global data on lake fetch may be less important. While using excessively large values of roughness lengths may degrade simulations, and lake geometry may influence lake temperature in other ways, model predictions were relatively insensitive even to extreme changes in the fetch from unlimited to 100 m. This low sensitivity may be because, using the Zilitinkevich et al. (2001) relationships, predicted scalar roughness lengths were relatively insensitive to changes in the momentum roughness length with fetch. However, we did not analyze changes in momentum flux, and it is unclear if these changes could be important in coupled simulations. In any case, retrieval of approximate lake horizontal dimensions from remote sensing should be relatively straightforward, so we still recommend the creation of a global dataset to eliminate this small source of uncertainty in global simulations.

4.5 Lake-Climate Interactions

Reducing surface roughness lengths and correcting errors in surface flux calculation reduced latent heat fluxes and delayed their seasonal peak in CLM4-LISSS compared to the existing CLM4 lake model, consistent with observations. While Bonan (1995) found large summer increases in latent heat fluxes at all latitudes when adding lakes to a GCM, the decreased roughness length and increased thermal inertia of lakes could tend to decrease latent heat fluxes compared to surrounding land area in the early summer, particularly at high latitudes, where there is large seasonal temperature variation and soil evaporation tends not to be moisture-limited. Samuelsson et al. (2010) found net regional summer warming resulting from lakes in Northern Europe. Dutra et al. (2010) found regional cooling at all latitudes, but increases in latent heat fluxes only occurred at low latitudes, while decreases occurred at high latitudes,

consistent with the findings of Lofgren (1997) for the Great Lakes and Krinner (2003) and Krinner and Boike (2010) for high latitudes. These results suggest that energy uptake by lakes may be more important than increasing latent heat fluxes as a summer cooling mechanism at temperate and high latitudes.

Studies tend to agree that lakes increase autumn heat fluxes and surface temperatures (Bonan 1995; Dutra et al. 2010; Lofgren 1997; Rouse et al. 2008; Samuelsson et al. 2010). In the winter, however, ice and snow model details are important. For example, studies tend to find that lakes cause warming when snow insulation is not modeled (Bonan 1995; Lofgren 1997; Samuelsson et al. 2010), while Dutra et al. (2010) found slight, if any, warming when snow insulation was present. (We note that the winter warming reported in Lofgren (1997) may be realistic, as the Great Lakes often do not completely freeze.) Krinner and Boike (2010), using a model with snow insulation, found that a fraction of the predicted autumn warming caused by lakes extended into the winter under present climate, while most of the autumn warming persisted into the winter under future climate; this discrepancy may be due to decreased snow thickness, but these results were not reported. The dependency on snow insulation of the winter atmospheric response to lakes is consistent with the large increases we found in winter energy fluxes from lakes to the atmosphere when eliminating snow insulation. We note that ignoring the heat of fusion caused half as large changes in flux but of the opposite sign, even though both changes tended to make lake ice surfaces colder in the winter: snow insulation keeps the lake ice from being exposed to cold atmospheric temperatures, while heat of fusion increases the thermal inertia of the lake itself.

Due to the potential for climate change to interact with thermokarst lake area (Smith et al. 2005), future studies should investigate the effects of these changes on regional climate (Krinner and Boike 2010). Other land cover change experiments have shown changes in atmospheric circulation or remote atmospheric conditions (Bala et al. 2007; Feddema et al. 2005a; Feddema et al. 2005b), but it is not clear if this could result from changing lake area. For studies showing increasing summer latent heat fluxes and surface cooling for regions with large lake area, it is unclear how this additional water vapor affected atmospheric conditions elsewhere. We address some of these questions in a related study (Subin et al., submitted to *Tellus A*).

Lake opacity may also interact with climate change, as both increasing opacity and increasing air temperatures can enhance summer stratification. Changes in climate and watershed properties can affect lake biology by changing temperature and the concentrations of dissolved nutrients and oxygen (Kosten et al. 2009; MacKay et al. 2009; Peeters et al. 2007; Verburg and Hecky 2009), and lake biology is a primary determinant of opacity (Cristofor et al. 1994). Like previous observational and modeling studies (Cristofor et al. 1994; Hocking and Straskraba 1999; Houser 2006; Mazumder and Taylor 1994; Mazumder et al. 1990; Persson and Jones 2008), we found that increased opacity increases summer stratification, and we also found large effects on surface energy fluxes. Although the extinction coefficient may be estimated using remote sensing or model inversions, these approaches will not be able to predict future changes in opacity under climate change or anthropogenic manipulation of watersheds. To do so would require explicitly modeling lake hydrology and biogeochemistry, including water and nutrient inputs, so that the lake water content, dissolved nutrient and oxygen concentrations, and biological activity can be predicted.

5. Conclusions

The existing CLM4 lake model performance was poor, with unrealistic predictions of water temperatures and surface fluxes for all four lakes simulated, likely attributable both to deficiencies in model structure and to errors in surface flux and lake temperature calculations (Sec. 7). The new CLM4 lake model (CLM4-LISSS) matched observations of water temperatures and surface fluxes very well for three small temperate and boreal lakes where local meteorological forcing observations were available. Biases in larger lakes were modest and comparable to those associated with uncertainty in lake characterizations (e.g., depth, opacity). Based on our analyses, we conclude that CLM4-LISSS is suitable for inclusion in global climate studies.

Neglecting the fact that lakes have much smaller effective aerodynamic roughness lengths than other land types represented in land surface models will lead to large biases in predicted surface fluxes and surface temperature. These resulting biases will be large compared to the effects of fetch and depth limitations on wave development.

Other missing processes in lake models or unavailable parameter data for global simulations can cause very large seasonal biases in local surface flux predictions of up to 30 W m^{-2}, highlighting needs for future research. Either neglecting snow insulation or the energy exchanges associated with phase change will lead to large declines in predicted winter lake ice temperatures, but with opposite effects on predicted surface fluxes and summer lake water temperatures. Observed lake opacity varies over more than two orders of magnitude, but even moderate variation in opacity caused larger changes in predicted surface fluxes than typical lake depth variation in our simulations. Consequently, global datasets of lake opacity should be developed based on remote sensing, and research should be undertaken to predict how lake optics might change under anthropogenic climate change and watershed manipulation. Decreases in frozen lake albedo during spring thaw can accelerate melt by a week or more at high latitudes, but current 1D model parameterizations are relatively crude.

Wind-driven eddy mixing predicted by the Hostetler Model was insufficient for simulating large lake surface fluxes and water temperatures; predictions were nearly always improved by increasing thermal conductivity by a large factor to account for unresolved 3D processes. Errors in surface fluxes that might result from insufficient mixing in large lakes were comparable to errors resulting from missing information on lake depth or opacity. Further research is needed to bridge the gap in model performance between small and large lakes for lake models coupled into climate models.

6. Acknowledgements

Andrey Martynov (Université du Québec à Montréal) provided processed data for Sparkling Lake (collected by the University of Wisconsin Center for Limnology) and important insight during model development. Victor Stepanenko (Moscow State University) provided processed data for Kossenblatter Lake (collected by the Lindenberg Meteorological Observatory and Richard Aßmann Observatory), helpful feedback during discussion of model results, and detailed comments on a draft manuscript. Marjorie Perroud (Switzerland Federal Office for the Environment) provided detailed comments on a draft manuscript. Annika Nordbo (University of Helsinki) provided processed data for Lake Valkea-Kotinen. Margaret Torn (Lawrence Berkeley National Laboratory) provided high-level guidance and advice. David Lawrence (National

Center for Atmospheric Research) provided support in using and modifying the CLM code and getting feedback from the CLM community. Two anonymous reviewers also provided helpful suggestions for revising the manuscript. This work was supported by the Director, Office of Science, Office of Biological and Environmental Research, Climate and Environmental Science Division, of the U.S. Department of Energy under Contract No. DE-AC02-05CH11231 to Berkeley Lab.

Author Attributions: Z.M.S. developed the model, designed experiments, and performed research. W.J.R. provided guidance during all stages of research. D.M. supported the formulation of the surface flux solution. Z.M.S. and W.J.R. wrote the paper, with comments from D.M.

7. Appendix: Deficiencies in the Existing CLM4 Lake Model

7.1 Comments on Model Formulation

In addition to the structural simplifications of the existing CLM4 lake model (e.g., lack of phase change and snow insulation), there are a number of unrealistic assumptions and errors in model formulation that contribute to the unphysical behavior of the model: an error in the eddy diffusivity calculation; the assumption that convection does not occur when the top of the lake is colder than freezing; excessively large surface roughness lengths; an error in the calculation of surface fluxes and surface temperature; and an unrealistic decoupling of the surface and the top water layer.

Two issues contribute to predictions in the existing CLM4 lake model of excessively mixed lakes in the summer and insufficiently mixed lakes in the winter. In the calculation of the wind-driven eddy diffusivity (Oleson et al. (2010), p. 184, Eq. 9-45), the equation is not corrected for the fact that the CLM4 code defines the z-coordinate as positive downwards while Hostetler and Bartlein (1990) define it as positive upwards. Thus, the square of the Brunt-Väisälä frequency is always calculated as negative and reset to zero by a flag in the code restricting it to be non-negative before a square root is taken. Consequently, the eddy diffusivity is always calculated as if the lake were perfectly neutrally stable, making the eddy diffusivity much larger than it should be when stable stratification occurs. In addition, the model does not allow convection to occur in the liquid portion of the lake when the top of the lake is colder than freezing, but this constraint is unphysical.

In the existing CLM4 lake model, the surface roughness lengths are set to constant values of 10 mm for unfrozen lakes and 40 mm for frozen lakes, which are much larger than values found in the literature for lakes, ocean, and sea ice. In Sec. 3.1.1, we showed that such large roughness lengths (in an otherwise unchanged CLM4-LISSS) yielded low surface temperatures, high latent heat fluxes, and low sensible heat fluxes during the summer over two lakes, as compared with observations.

An error and an unrealistic assumption in the calculation of surface fluxes tend to decrease water temperatures, increase latent heat fluxes, and increase diurnal surface temperature variation. In both the existing CLM4 lake model and CLM4-LISSS, Eq. 13 is solved using the Newton-Raphson method:

$$\Delta T_g = \frac{S + L - H - \lambda E - G}{-\frac{\partial L}{\partial T_g} + \frac{\partial H}{\partial T_g} + \lambda \frac{\partial E}{\partial T_g} + \frac{\partial G}{\partial T_g}}, \qquad \textbf{Eq. 16}$$

where ΔT_g is the change in predicted surface temperature between iterations. However, in the existing CLM4 lake model [Eq. 9.10 on p. 176 in Oleson et al. (2010)], the term S corresponds to the *total* absorbed shortwave radiation for the lake, *not* the fraction absorbed at the surface (as is used in Eq. 14 here). Energy is still conserved, as the correct expression is used when calculating G, which is then used as the top boundary condition for the temperature solution of the lake body. However, this tends to increase the surface temperature and heat fluxes during the daytime at the expense of energy entering the lake. In addition, the thermal conductance between the surface and the top model layer only includes molecular diffusivity, which will be several orders of magnitude smaller than the eddy diffusivity for unfrozen lakes. Moreover, the surface temperature T_g is not corrected for convection within the top lake layer when the calculated T_g implies an unstable density profile in the top lake layer. These two assumptions create an unrealistic decoupling between the surface and the top lake layer, hiding the effect of the error in S during the daytime but also allowing for unrealistically low night-time and autumn surface temperatures and large daily temperature variability.

7.2 Unphysical Behavior of the Existing CLM4 Lake Model Compared to Observations

The issues described above have a synergistic effect in producing excessively cold, well-mixed lakes with excessive latent heat flux, insufficient or negative sensible heat flux, low night-

time and autumn surface temperatures, and excessive surface temperature variability. These effects were evident in Sparkling Lake (Sec. 3.1.1) and all three other lakes where the existing CLM4 lake model was evaluated. The simulated Lake Michigan remained well-mixed (not shown) at a constant temperature during the entire unfrozen season (Supp. Fig. 8). Summer near-surface water temperatures were too cold, and the lack of phase change and the suppression of convection for lakes with surface temperature below freezing contributed to unrealistic autumn temperature variability and a sometimes unstable vertical temperature profile. The surface and 0.05 m water temperatures are shown separately to illustrate their unrealistic decoupling; the simulated surface temperature had unrealistically large daily variability and tended to closely follow the air temperature (not shown), seasonally leading both the observed and simulated lake near-surface temperatures. The simulation of Great Slave Lake yielded an early summer peak in both latent and sensible heat fluxes, insufficient summer stratification, a very early initial autumn surface freeze-up, and unrealistic autumn near-surface water temperature variability with a sometimes unstable vertical temperature profile (Supp. Fig. 9). The surface temperature showed the same unphysical behavior as for Lake Michigan. Lake McIlwaine was predicted to be well-mixed throughout the year with little seasonal temperature variation, inconsistent with observations (Supp. Fig. 7c-d).

Figures

Fig. 1: Lake model schematic.

Fig. 2: Daily mean Sparkling Lake water temperatures and 30-day mean surface energy fluxes, 2002-2005, observed, simulated by CLM4-LISSS, and simulated by the existing CLM4 lake model: (a) 0.05 m water temperature (below-freezing temperatures are not shown, as surface observations are typically flawed during these periods); (b) water temperature at 10 m depth; (c) latent heat flux; and (d) sensible heat flux.

Fig. 3: Ten-day mean Sparkling Lake (a) 0.05 m temperature and (b) latent heat flux, 2002-2005, observed and simulated by CLM4-LISSS with diagnostic roughness lengths, fixed 1 mm roughness lengths, and fixed 10 mm roughness lengths. Near-surface below-freezing temperatures are not shown, as surface observations are typically flawed during these periods.

Fig. 4: Five-day mean Kossenblatter water temperatures and surface energy fluxes, May – November, 2003, observed and simulated by CLM4-LISSS with diagnostic roughness lengths, fixed 1 mm roughness lengths, and fixed 10 mm roughness lengths: (a) surface temperature; (b) temperature at 1 m depth; (c) latent heat flux; and (d) sensible heat flux.

Fig. 5: Lake Valkea-Kotinen, May – December, 2006. Ten-day mean water temperatures: (a) observed (Nordbo et al. 2011); and (b) simulated by CLM4-LISSS. Three-day mean (over available data for the sporadic observations) 12-6 PM surface energy fluxes, observed and simulated: (c) latent heat flux; and (d) sensible heat flux.

Fig. 6: Snow thickness and ice thickness, simulated by CLM4-LISSS and observed, for (a) Big Island Lake; (b) Lake Gogebic; (c) Ryan Lake (Gu and Stefan 1993); and (d) Thrush Lake (Fang and Stefan 1996).

Fig. 7: Daily mean Lake Michigan water temperatures for 1990: (a) CLM4-LISSS; (b) CLM4-LISSS with non-molecular diffusivity increased by 10; and (c) observed (McCormick and Pazdalski 1993).

Fig. 8: Daily mean Lake Michigan surface temperatures for 1990: National Data Buoy Center Station 45007 observations, National Data Buoy Center Station 45002 observations, and simulated by CLM4-LISSS, CLM4-LISSS with non-molecular diffusivity increased by 10, and CLM4-LISSS with no enhanced diffusion.

Fig. 9: Daily-averaged Great Slave Lake water temperatures and surface fluxes from 1997-2003 excluding 2001, observed (Rouse et al. 2008) and simulated by CLM4-LISSS, CLM4-LISSS with no enhanced diffusion, and CLM4-LISSS with non-molecular diffusivity increased by 100: (a) surface temperature; (b) temperature at 40 m depth; (c) latent heat; and (d) sensible heat.

Fig. 10: Monthly average surface flux anomalies for North Eurasian (60 – 90°N, 0 – 175°E) lakes, latent heat, sensible heat, rate of lake enthalpy decrease, and upward longwave: (a) Case 2, no snow insulation; (b) Case 1, no heat of fusion for phase change; (c) Case 6, lake depth = 5 m; and (d) Case 5, lake depth = 50 m.

Fig. 11: Monthly average water temperatures for the gridcell co-located with Finnish Lake Inari: (a) Case 0, baseline; (b) Case 2, no snow insulation; (c) Case 7, extinction coefficient = 1.0 m^{-1}; and (d) Case 13, non-molecular diffusivities increased by 10.

Fig. 12: Monthly average surface flux anomalies for North Eurasian (60 – 90°N, 0 – 175°E) lakes, latent heat, sensible heat, rate of lake enthalpy decrease, and upward longwave: (a) Case 7, extinction coefficient = 1.0 m^{-1}; (b) Case 11, no albedo correction for melting lakes; (c) Case 8, roughness lengths = 1 mm; and (d) Case 13, non-molecular diffusivities increased by 10.

Supplemental Figures (to be provided in the Supplementary Information; captions are only included here for linking with the text and for review and should be removed when in press)

Supp. Fig. 1: (a) % lake area used in this study (Lehner and Doll 2004) , and (b-d) comparison of gridded lake depth (m) interpolated from 1 km resolution in Kourzeneva et al. (2010) to 1.9 x 2.5° resolution used in CLM with alternative interpolation approaches: (b) mean depth of all lakes (weighted by fraction of 1 km gridcells); (c) mode depth of lakes in 1 km gridcells; (d) mean depth of all lakes for which real data were available, rather than the default 10 m.

Supp. Fig. 2: Lake Karujärv, 1979-1988: (a) surface temperature; (b) snow and ice thickness.

Supp. Fig. 3: Thrush Lake water temperatures, 1986-1991: (a) 1 m; (b) 7 m.

Supp. Fig. 4: Lake Raksjo water temperatures, 1995: surface, 5 m, and 9.5 m.

Supp. Fig. 5: Crater Lake 1988-2000 monthly-averaged water temperatures, simulated by CLM4-LISSS, CLM4-LISSS with non-molecular diffusivities increased by 10, and observed (Larson et al. 2007), for mean January and mean July.

Supp. Fig. 6: Crater Lake 1988-2000 monthly averaged surface temperature, simulated by CLM4-LISSS, observed (Larson et al. 2007), CLM4-LISSS with non-molecular diffusivities increased by 10, and CLM4-LISSS without enhanced diffusion.

Supp. Fig. 7: Lake McIlwaine water temperatures for 11 Aug. 1975, 28 Oct. 1975, and 11 Feb. 1976: (a) simulated by CLM4-LISSS; (b) simulated by CLM4-LISSS with non-molecular diffusivities increased by 10; (c) observed (Robarts and Ward 1978); and (d) simulated by the existing CLM4.

Supp. Fig. 8: Daily mean Lake Michigan near-surface temperatures for 1990: National Data Buoy Center Station 45007 observations, National Data Buoy Center Station 45002 observations, simulated by the existing CLM4 (surface temperature), and simulated by the existing CLM4 (0.05 m temperature).

Supp. Fig. 9: Daily-averaged Great Slave Lake water temperatures and surface fluxes from 1997-2003 excluding 2001, observed (Rouse et al. 2008) and simulated by the existing CLM4: (a) near-surface temperature; (b) temperature at 40 m depth; (c) latent heat; and (d) sensible heat.

Supp. Fig. 10: Monthly average surface flux anomalies for North Eurasian (60 – 90°N, 0 – 175°E) lakes: Cases 1-4.

Supp. Fig. 11: Monthly average surface flux anomalies for North Eurasian (60 – 90°N, 0 – 175°E) lakes: Cases 5-8.

Supp. Fig. 12: Monthly average surface flux anomalies for North Eurasian (60 – 90°N, 0 – 175°E) lakes: Cases 9-12.

Supp. Fig. 13: Monthly average surface flux anomalies for North Eurasian (60 – 90°N, 0 – 175°E) lakes: Cases 13-14.

Supp. Fig. 14: Monthly average water temperatures for the gridcell co-located with Finnish Lake Inari: Cases 0-3 (Case 0 is the baseline).

Supp. Fig. 15: Monthly average water temperatures for the gridcell co-located with Finnish Lake Inari: Cases 4-6.

Supp. Fig. 16: Monthly average water temperatures for the gridcell co-located with Finnish Lake Inari: Cases 7-9.

Supp. Fig. 17: Monthly average water temperatures for the gridcell co-located with Finnish Lake Inari: Cases 10-12.

Supp. Fig. 18: Monthly average water temperatures for the gridcell co-located with Finnish Lake Inari: Cases 13-14.

Tables

Table 1: Simulated Lakes

Name	*Location (°N, °E)*	*Depth (m)*	*η (m^{-1})*	*Fetch (km)*	*Forcing*	*Spinup (yr)*	*Evaluation Period*	*Variables Evaluated*	*References*
Sparkling	46.01, -89.70	18	0.27	0.5	Obs.	5	2002-2005	WT, SF	(Martynov et al. 2010); lter.limnology.wisc.edu
Kossenblatter	52.13, 14.1	2	7.08	1.0	Obs.	5	05/2003-11/2003	WT, SF, ST	(Beyrich et al. 2006); Stepanenko et al., submitted to *Tellus A*; Lindenberg Meteorological Observatory, Richard Aßmann Observatory, DWD, Germany
Valkea-Kotinen	61.24, 25.06	6	3.1	0.3	Obs.	2	05/2006-12/2006	WT, SF	(Nordbo et al. 2011; Vesala et al. 2006); www.atm.helsinki.fi
Michigan	44, -87	160	N/A	60	NCEP	40	04/1990-12/1990	WT, ST	(McCormick and Pazdalski 1993); www.ndbc.noaa.gov (Stat. 45002, 45007)[‡]
Great Slave	61.6, -114.0	90	N/A	65	NCEP	40	1997-2003	WT, SF	(Rouse et al. 2008)
Ryan	45.04, -93.32	11	0.5	0.2	NCEP	9	1989-1990	IsT	(Gu and Stefan 1993)
Thrush	47.90, -90.50	14	0.45	0.2	NCEP	10	1986-1991	WT, IsT	(Fang and Stefan 1996)
Big Island	46.18, -86.50	11	N/A	0.2	NCEP	8	1968	IsT	(Sleator 1995); nsidc.org/data/g00803.html

									(Stat. 210)
Gogebic	46.60, -89.58	5	N/A	3.0	NCEP	7	1968-1970	IsT	(Sleator 1995); nsidc.org/data/g00803.html (Stat. 128)
Karujärv	58.38, 22.22	2	2.0	0.15	NCEP	3	1979-1987	WT, IsT	(Vassiljev et al. 1994)
Raksjo	60.03, 17.08	10	0.54	0.6	NCEP	4	05/1995-09/1995	WT, ST	(Elo 2007)
Crater	42.93, -122.10	500	0.05	4.0	NCEP†	64**	1988-2000	WT	(Larson et al. 2007)
McIlwaine*	-17.90, 30.80	25	N/A	2.0	NCEP	45	08/1975-02/1976	WT	(Robarts and Ward 1978)

Notes. **McIlwaine*: Now appears to be part of Zimbabwe and renamed Lake Chivero. *Depth*: The depth used for simulation, which is the mean depth, the maximum depth, or the depth at the measurement site. η: The extinction coefficient used for simulation; N/A means the default depth-based expression based on Hakanson (1995) was used. *Forcing*: NCEP = 2° global reanalysis data processed for CESM (1948-2004) (Qian et al. 2006). †Because Crater Lake is about 900 m above the forcing gridcell average altitude, we subtracted 6°C from the forcing temperature and 7500 Pa from the forcing pressure. ***Spinup*: Crater Lake was spun up for 25 years (1948-1972) with 10,000 times increased thermal conductivity before 39 years of conventional spinup. *Variables evaluated*: WT = water temperature; SF = surface fluxes; ST = surface temperature; IsT = ice & snow thickness. We note that a short period of data on sediment temperatures was available in Gu and Stefan (1993), but this data were insufficient to effectively evaluate CLM4-LISSS in the absence of more detailed data (e.g., sediment characteristics, near-lake meteorological conditions). ‡*References*: for Lake Michigan, these 2 buoys were selected because they were located mid-lake and relatively close to the simulated point corresponding to the McCormick and Pazdalski (1993) observations; several other buoys were located on the shoreline.

References

Ahrens, T. J., 1995: *Rock physics & phase relations : a handbook of physical constants.* American Geophysical Union.

Anctil, F., and M. A. Donelan, 1996: Air-water momentum flux observations over shoaling waves. *J. Phys. Oceanogr.*, **26,** 1344-1353.

Andreas, E. L., 1987: A Theory For The Scalar Roughness and the Scalar Transfer-Coefficients over Snow and Sea Ice. *Boundary-Layer Meteorology*, **38,** 159-184.

Arp, C. D., B. M. Jones, F. E. Urban, and G. Grosse, 2011: Hydrogeomorphic processes of thermokarst lakes with grounded-ice and floating-ice regimes on the Arctic coastal plain, Alaska. *Hydrological Processes*, **25,** 2422-2438.

Atakturk, S. S., and K. B. Katsaros, 1999: Wind stress and surface waves observed on Lake Washington. *J. Phys. Oceanogr.*, **29,** 633-650.

Bala, G., K. Caldeira, M. Wickett, T. J. Phillips, D. B. Lobell, C. Delire, and A. Mirin, 2007: Combined climate and carbon-cycle effects of large-scale deforestation. *Proceedings of the National Academy of Sciences of the United States of America*, **104,** 6550-6555.

Balsamo, G., E. Dutra, V. M. Stepanenko, P. Viterbo, P. M. A. Miranda, and D. Mironov, 2010: Deriving an effective lake depth from satellite lake surface temperature data: a feasibility study with MODIS data. *Boreal Environment Research*, **15,** 178-190.

Bates, G. T., F. Giorgi, and S. W. Hostetler, 1993: Towards the Simulation of the Effects of the Great-Lakes on Regional Climate. *Mon. Weather Rev.*, **121,** 1373-1387.

Beyrich, F., and Coauthors, 2006: Area-averaged surface fluxes over the litfass region based on eddy-covariance measurements. *Boundary-Layer Meteorology*, **121,** 33-65.

Blenckner, T., A. Omstedt, and M. Rummukainen, 2002: A Swedish case study of contemporary and possible future consequences of climate change on lake function. *Aquat. Sci.*, **64,** 171-184.

Bonan, G., 1998: The land surface climatology of the NCAR Land Surface Model coupled to the NCAR Community Climate Model. *J. Clim.*, **11,** 1307-1326.

Bonan, G., S. Levis, L. Kergoat, and K. Oleson, 2002a: Landscapes as patches of plant functional types: An integrating concept for climate and ecosystem models. *Global Biogeochemical Cycles*, **16,** -.

Bonan, G. B., 1995: Sensitivity of a GCM Simulation to Inclusion of Inland Water Surfaces. *J. Clim.*, **8,** 2691-2704.

Bonan, G. B., and Coauthors, 2002b: The land surface climatology of the community land model coupled to the NCAR community climate model. *Journal of Climate*, **15,** 3123-3149.

Brown, L. C., and C. R. Duguay, 2010: The response and role of ice cover in lake-climate interactions. *Prog. Phys. Geogr.*, **34,** 671-704.

Cardille, J., S. Carpenter, J. Foley, P. Hanson, M. Turner, and J. Vano, 2009: Climate change and lakes: Estimating sensitivities of water and carbon budgets. *Journal of Geophysical Research-Biogeosciences*, **114,** -.

Charnock, H., 1955: Wind Stress Over a Water Surface. *Quart. J. Roy. Meteorol. Soc.*, **81,** 639-640.

Cristofor, S., A. Vadineanu, G. Ignat, and C. Ciubuc, 1994: Factors Affecting Light Penetration in Shallow Lakes. *Hydrobiologia*, **275,** 493-498.

Dai, Y. J., and Coauthors, 2003: The Common Land Model. *Bulletin of the American Meteorological Society*, **84,** 1013-.

Donelan, M. A., F. W. Dobson, S. D. Smith, and R. J. Anderson, 1993: On the Dependence of Sea-Surface Roughness on Wave Development. *J. Phys. Oceanogr.*, **23,** 2143-2149.

Downing, J. A., and Coauthors, 2006: The global abundance and size distribution of lakes, ponds, and impoundments. *Limnology and Oceanography*, **51,** 2388-2397.

Duarte, C. M., Y. T. Prairie, C. Montes, J. J. Cole, R. Striegl, J. Melack, and J. A. Downing, 2008: CO2 emissions from saline lakes: A global estimate of a surprisingly large flux. *Journal of Geophysical Research-Biogeosciences*, **113**.

Dutra, E., V. M. Stepanenko, G. Balsamo, P. Viterbo, P. M. A. Miranda, D. Mironov, and C. Schar, 2010: An offline study of the impact of lakes on the performance of the ECMWF surface scheme. *Boreal Environment Research*, **15,** 100-112.

Ellis, C. R., H. G. Stefan, and R. Gu, 1991: Water Temperature Dynamics and Heat-Transfer Beneath the Ice Cover of a Lake. *Limnology and Oceanography*, **36,** 324-335.

Elo, P. A. R., 2007: The energy balance and vertical thermal structure of two small boreal lakes in summer. *Boreal Environment Research*, **12,** 585-600.

Fairall, C. W., E. F. Bradley, D. P. Rogers, J. B. Edson, and G. S. Young, 1996: Bulk parameterization of air-sea fluxes for Tropical Ocean Global Atmosphere Coupled Ocean Atmosphere Response Experiment. *J. Geophys. Res.-Oceans*, **101,** 3747-3764.

Fang, X., and H. G. Stefan, 1996: Long-term lake water temperature and ice cover simulations/measurements. *Cold Reg. Sci. Tech.*, **24,** 289-304.

Fang, X., and H. G. Stefan, 1998: Temperature variability in lake sediments. *Water Resources Research*, **34,** 717-729.

Fang, X., and H. G. Stefan, 2009: Simulations of climate effects on water temperature, dissolved oxygen, and ice and snow covers in lakes of the contiguous United States under past and future climate scenarios. *Limnology and Oceanography*, **54,** 2359-2370.

Farouki, O. T., 1981: The Thermal-Properties of Soils in Cold Regions. *Cold Reg. Sci. Tech.*, **5,** 67-75.

Feddema, J., K. Oleson, G. Bonan, L. Mearns, W. Washington, G. Meehl, and D. Nychka, 2005a: A comparison of a GCM response to historical anthropogenic land cover change and model sensitivity to uncertainty in present-day land cover representations. *Climate Dynamics*, **25,** 581-609.

Feddema, J. J., K. W. Oleson, G. B. Bonan, L. O. Mearns, L. E. Buja, G. A. Meehl, and W. M. Washington, 2005b: The importance of land-cover change in simulating future climates. *Science*, **310,** 1674-1678.

Flanner, M. G., and C. S. Zender, 2006: Linking snowpack microphysics and albedo evolution. *Journal of Geophysical Research-Atmospheres*, **111**.

Flanner, M. G., C. S. Zender, J. T. Randerson, and P. J. Rasch, 2007: Present-day climate forcing and response from black carbon in snow. *Journal of Geophysical Research-Atmospheres*, **112**.

Foken, T., 2008: The energy balance closure problem: An overview. *Ecological Applications*, **18,** 1351-1367.

Freilich, M. H., and R. T. Guza, 1984: Nonlinear Effects on Shoaling Surface Gravity-Waves. *Philos. Trans. R. Soc. Lond. Ser. A-Math. Phys. Eng. Sci.*, **311,** 1-41.

Freilich, M. H., R. T. Guza, and S. L. Elgar, 1990: Observations of Nonlinear Effects in Directional Spectra of Shoaling Gravity-Waves. *J. Geophys. Res.-Oceans*, **95,** 9645-9656.

Gao, Z. Q., Q. Wang, and M. Y. Zhou, 2009: Wave-Dependence of Friction Velocity, Roughness Length, and Drag Coefficient over Coastal and Open Water Surfaces by Using Three Databases. *Adv. Atmos. Sci.*, **26,** 887-894.

Gebhart, B., and J. C. Mollendorf, 1977: New Density Relation for Pure and Saline Water. *Deep-Sea Research*, **24,** 831-848.

Geernaert, G. L., S. E. Larsen, and F. Hansen, 1987: Measurements of the Wind-Stress, Heat-Flux, and Turbulence Intensity During Storm Conditions over the North-Sea. *J. Geophys. Res.-Oceans*, **92,** 13127-13139.

Gent, P. R., and Coauthors, 2011: The Community Climate System Model Version 4. *J. Climate***,** doi: 10.1175/2011JCLI4083.1

Golosov, S., and G. Kirillin, 2010: A parameterized model of heat storage by lake sediments. *Environmental Modelling & Software*, **25,** 793-801.

Gomez, J. A. D., E. C. Salinero, and A. S. Merlin, 2009: Monitoring transparency in inland water bodies using multispectral images. *Int. J. Remote Sens.*, **30,** 1567-1586.

Goudsmit, G. H., H. Burchard, F. Peeters, and A. Wuest, 2002: Application of k-epsilon turbulence models to enclosed basins: The role of internal seiches. *J. Geophys. Res.-Oceans*, **107,** 13.

Goyette, S., N. McFarlane, and G. Flato, 2000: Application of the Canadian Regional Climate Model to the Laurentian Great Lakes region: Implementation of a lake model. *Atmosphere-Ocean*, **38,** 481-503.

Gu, R. C., and H. G. Stefan, 1993: Validation of Cold Climate Lake Temperature Simulation. *Cold Reg. Sci. Tech.*, **22,** 99-104.

Hagemann, S., K. Arpe, and E. Roeckner, 2006: Evaluation of the hydrological cycle in the ECHAM5 model. *Journal of Climate*, **19,** 3810-3827.

Hakanson, L., 1995: Models to Predict Secchi Depth in Small Glacial Lakes. *Aquat. Sci.*, **57,** 31-53.

Hazewinkel, M., 1995: *Encyclopaedia of mathematics : an updated and annotated translation of the Soviet "Mathematical Encyclopaedia"*. Kluwer.

Hocking, G. C., and M. Straskraba, 1999: The effect of light extinction on thermal stratification in reservoirs and lakes. *International Review of Hydrobiology*, **84,** 535-556.

Hondzo, M., and H. G. Stefan, 1993: Lake Water Temperature Simulation-Model. *J. Hydraul. Eng.-ASCE*, **119,** 1251-1273.

Hostetler, S., and P. Bartlein, 1990: Simulation of Lake Evaporation with Application to Modeling Lake Level Variations of Harney-Malheur Lake, Oregon. *Water Resources Research*, **26,** 2603-2612.

Houser, J. N., 2006: Water color affects the stratification, surface temperature, heat content, and mean epilimnetic irradiance of small lakes. *Canadian Journal of Fisheries and Aquatic Sciences*, **63,** 2447-2455.

Hutchinson, G. E., 1957: *A treatise on limnology: Geography, Physics and Chemistry.* Vol. 1, Wiley.

Idso, S. B., and R. G. Gilbert, 1974: On the Universality of the Poole and Atkins Secchi Disk-Light Extinction Equation. *Journal of Applied Ecology*, **11,** 399-401.

Jeffries, M., T. Zhang, K. Frey, and N. Kozlenko, 1999: Estimating late-winter heat flow to the atmosphere from the lake-dominated Alaskan North Slope. *J. Glaciol.*, **45,** 315-324.

Jin, J., X. Gao, Z. Yang, R. Bales, S. Sorooshian, and R. Dickinson, 1999: Comparative analyses of physically based snowmelt models for climate simulations. *J. Clim.*, **12,** 2643-2657.

King, J. R., B. J. Shuter, and A. P. Zimmerman, 1997: The response of the thermal stratification of South Bay (Lake Huron) to climatic variability. *Canadian Journal of Fisheries and Aquatic Sciences*, **54,** 1873-1882.

Kirillin, G., 2010: Modeling the impact of global warming on water temperature and seasonal mixing regimes in small temperate lakes. *Boreal Environment Research*, **15,** 279-293.

Koponen, S., J. Pulliainen, K. Kallio, and M. Hallikainen, 2002: Lake water quality classification with airborne hyperspectral spectrometer and simulated MERIS data. *Remote Sens. Environ.*, **79,** 51-59.

Kosten, S., V. L. M. Huszar, N. Mazzeo, M. Scheffer, L. D. L. Sternberg, and E. Jeppesen, 2009: Lake and watershed characteristics rather than climate influence nutrient limitation in shallow lakes. *Ecological Applications*, **19,** 1791-1804.

Kourzeneva, E., 2010: External data for lake parameterization in Numerical Weather Prediction and climate modeling. *Boreal Environment Research*, **15,** 165-177.

Krinner, G., 2003: Impact of lakes and wetlands on boreal climate. *Journal of Geophysical Research-Atmospheres*, **108,** 18.

Krinner, G., and J. Boike, 2010: A study of the large-scale climatic effects of a possible disappearance of high-latitude inland water surfaces during the 21st century. *Boreal Environment Research*, **15,** 203-217.

Kristovich, D. A. R., and R. R. Braham, 1998: Mean profiles of moisture fluxes in snow-filled boundary layers. *Boundary-Layer Meteorology*, **87,** 195-215.

Laird, N. F., J. Desrochers, and M. Payer, 2009: Climatology of Lake-Effect Precipitation Events over Lake Champlain. *J. Appl. Meteorol. Climatol.*, **48,** 232-250.

Larson, G. L., R. L. Hoffman, D. C. McIntire, M. W. Buktenica, and S. F. Girdner, 2007: Thermal, chemical, and optical properties of Crater Lake, Oregon. *Hydrobiologia*, **574,** 69-84.

Lawrence, D. M., and A. G. Slater, 2008: Incorporating organic soil into a global climate model. *Climate Dynamics*, **30,** 145-160.

Lawrence, D. M., A. G. Slater, V. E. Romanovsky, and D. J. Nicolsky, 2008: Sensitivity of a model projection of near-surface permafrost degradation to soil column depth and representation of soil organic matter. *Journal of Geophysical Research-Earth Surface*, **113,** 14.

Lawrence, D. M., and Coauthors, 2011: Parameterization improvements and functional and structural advances in version 4 of the Community Land Model. *J. Adv. Model. Earth Sys.*, **3,** 1.

Lehner, B., and P. Doll, 2004: Development and validation of a global database of lakes, reservoirs and wetlands. *Journal of Hydrology*, **296,** 1-22.

Leon, L. F., D. C. L. Lam, W. M. Schertzer, D. A. Swayne, and J. Imberger, 2007: Towards coupling a 3D hydrodynamic lake model with the Canadian Regional Climate Model: Simulation on Great Slave Lake. *Environmental Modelling & Software*, **22,** 787-796.

Lofgren, B. M., 1997: Simulated effects of idealized Laurentian Great Lakes on regional and large-scale climate. *J. Clim.*, **10,** 2847-2858.

Lofgren, B. M., 2004: A model for simulation of the climate and hydrology of the Great Lakes basin. *Journal of Geophysical Research-Atmospheres*, **109**.

Long, Z., W. Perrie, J. Gyakum, D. Caya, and R. Laprise, 2007: Northern lake impacts on local seasonal climate. *J. Hydrometeorol.*, **8,** 881-896.

Maat, N., C. Kraan, and W. A. Oost, 1991: The Roughness of Wind-Waves. *Boundary-Layer Meteorology*, **54,** 89-103.

MacKay, M. D., and Coauthors, 2009: Modeling lakes and reservoirs in the climate system. *Limnology and Oceanography*, **54,** 2315-2329.

Mahrt, L., 1999: The Coastal Zone. *Air-Sea Exchange: Physics, Chemistry, and Dynamics*, G. L. Geernaert, Ed., Kluwer Academic Publishers, 247-267.

Martynov, A., L. Sushama, and R. Laprise, 2010: Simulation of temperate freezing lakes by one-dimensional lake models: performance assessment for interactive coupling with regional climate models. *Boreal Environment Research*, **15,** 143-164.

Mazumder, A., and W. D. Taylor, 1994: Thermal Structure of Lakes Varying in Size and Water Clarity. *Limnology and Oceanography*, **39,** 968-976.

Mazumder, A., W. D. Taylor, D. J. McQueen, and D. R. S. Lean, 1990: Effects of Fish and Plankton on Lake Temperature and Mixing Depth. *Science*, **247,** 312-315.

McCormick, M., and J. Pazdalski, 1993: Monitoring Midlake Water Temperature in Southern Lake-Michigan for Climate-Change Studies. *Clim. Change*, **25,** 119-125.

McCormick, M. J., and G. L. Fahnenstiel, 1999: Recent climatic trends in nearshore water temperatures in the St. Lawrence Great Lakes. *Limnology and Oceanography*, **44,** 530-540.

Mironov, D., L. Rontu, E. Kourzeneva, and A. Terzhevik, 2010a: Towards improved representation of lakes in numerical weather prediction and climate models: Introduction to the special issue of Boreal Environment Research. *Boreal Environment Research*, **15,** 97-99.

Mironov, D., A. Terzhevik, G. Kirillin, T. Jonas, J. Malm, and D. Farmer, 2002: Radiatively driven convection in ice-covered lakes: Observations, scaling, and a mixed layer model. *J. Geophys. Res.-Oceans*, **107,** 16.

Mironov, D., E. Heise, E. Kourzeneva, B. Ritter, N. Schneider, and A. Terzhevik, 2010b: Implementation of the lake parameterisation scheme FLake into the numerical weather prediction model COSMO. *Boreal Environment Research*, **15,** 218-230.

Morris, E. M., 1989: Turbulent Transfer over Snow and Ice. *Journal of Hydrology*, **105,** 205-223.

Mueller, D. R., P. Van Hove, D. Antoniades, M. O. Jeffries, and W. F. Vincent, 2009: High Arctic lakes as sentinel ecosystems: Cascading regime shifts in climate, ice cover, and mixing. *Limnology and Oceanography*, **54,** 2371-2385.

Nordbo, A., S. Launiainen, I. Mammarella, M. Lepparanta, J. Huotari, A. Ojala, and T. Vesala, 2011: Long-term energy flux measurements and energy balance over a small boreal lake using eddy covariance technique. *Journal of Geophysical Research-Atmospheres*, **116**.

Oleson, K., and Coauthors, 2010: Technical description of version 4.0 of the Community Land Model (CLM). National Center for Atmospheric Research, NCAR/TN-478+STR. http://www.cesm.ucar.edu/models/ccsm4.0/clm/CLM4_Tech_Note.pdf

Panin, G. N., A. E. Nasonov, T. Foken, and H. Lohse, 2006: On the parameterisation of evaporation and sensible heat exchange for shallow lakes. *Theoretical and Applied Climatology*, **85,** 123-129.

Peeters, F., D. Straile, A. Lorke, and D. M. Livingstone, 2007: Earlier onset of the spring phytoplankton bloom in lakes of the temperate zone in a warmer climate. *Glob. Change Biol.*, **13,** 1898-1909.

Perroud, M., and S. Goyette, 2010: Impact of warmer climate on Lake Geneva water-temperature profiles. *Boreal Environment Research*, **15,** 255-278.

Perroud, M., S. Goyette, A. Martynov, M. Beniston, and O. Anneville, 2009: Simulation of multiannual thermal profiles in deep Lake Geneva: A comparison of one-dimensional lake models. *Limnology and Oceanography*, **54,** 1574-1594.

Persson, I., and I. D. Jones, 2008: The effect of water colour on lake hydrodynamics: a modelling study. *Freshw. Biol.*, **53,** 2345-2355.

Pivovarov, A. A., 1972: *Thermal Conditions in Freezing Lakes and Reservoirs.* John Wiley.

Plummer, D. A., and Coauthors, 2006: Climate and climate change over North America as simulated by the Canadian RCM. *J. Clim.*, **19,** 3112-3132.

Qian, T. T., A. G. Dai, K. E. Trenberth, and K. W. Oleson, 2006: Simulation of global land surface conditions from 1948 to 2004. Part I: Forcing data and evaluations. *J. Hydrometeorol.*, **7,** 953-975.

Robarts, R. D., and P. R. B. Ward, 1978: Vertical Diffusion and Nutrient Transport in a Tropical Lake (Lake McIlwaine, Rhodesia). *Hydrobiologia*, **59,** 213-221.

Rouse, W. R., P. D. Blanken, N. Bussieres, C. J. Oswald, W. M. Schertzer, C. Spence, and A. E. Walker, 2008: Investigation of the Thermal and Energy Balance Regimes of Great Slave and Great Bear Lakes. *J. Hydrometeorol.*, **9,** 1318-1333.

Rouse, W. R., and Coauthors, 2005: The role of northern lakes in a regional energy balance. *J. Hydrometeorol.*, **6,** 291-305.

Saloranta, T. M., M. Forsius, M. Jarvinen, and L. Arvola, 2009: Impacts of projected climate change on the thermodynamics of a shallow and a deep lake in Finland: model simulations and Bayesian uncertainty analysis. *Hydrol. Res.*, **40,** 234-248.

Samuelsson, P., and M. Tjernstrom, 2001: Mesoscale flow modification induced by land-lake surface temperature and roughness differences. *Journal of Geophysical Research-Atmospheres*, **106,** 12419-12435.

Samuelsson, P., E. Kourzeneva, and D. Mironov, 2010: The impact of lakes on the European climate as simulated by a regional climate model. *Boreal Environment Research*, **15,** 113-129.

Schindler, D. W., 2009: Lakes as sentinels and integrators for the effects of climate change on watersheds, airsheds, and landscapes. *Limnology and Oceanography*, **54,** 2349-2358.

Skamarock, W. C., and Coauthors, 2008: A Description of the Advanced Research WRF Version 3. Mesoscale and Microscale Meteorology Division, National Center for Atmospheric Research, NCAR/TN–475+STR. http://www.mmm.ucar.edu/wrf/users/docs/arw_v3.pdf

Sleator, F. E., 1995: GLERL Great Lakes ice thickness data base, 1966-1979. National Snow and Ice Data Center. http://www.glerl.noaa.gov/data/pgs/ice.html

Small, E. E., F. Giorgi, L. C. Sloan, and S. Hostetler, 2001: The effects of desiccation and climatic change on the hydrology of the Aral Sea. *J. Clim.*, **14,** 300-322.

Smith, L., Y. Sheng, G. MacDonald, and L. Hinzman, 2005: Disappearing Arctic lakes. *Science*, **308,** 1429-1429.

Smith, S. D., 1988: Coefficients for Sea-Surface Wind Stress, Heat-Flux, and Wind Profiles as a Function of Wind-Speed and Temperature. *J. Geophys. Res.-Oceans*, **93,** 15467-15472.

Smith, S. D., and Coauthors, 1992: Sea-Surface Wind Stress and Drag Coefficients - The HEXOS Results. *Boundary-Layer Meteorology*, **60,** 109-142.

Song, Y., F. H. M. Semazzi, L. Xie, and L. J. Ogallo, 2004: A coupled regional climate model for the Lake Victoria basin of East Africa. *Int. J. Climatol.*, **24,** 57-75.

Stepanenko, V. M., and V. N. Lykossov, 2005: Numerical modeling of heat and moisture transfer processes in a system lake – soil. *Russian Journal for Meteorology and Hydrology*, **3,** 95-104.

Stepanenko, V. M., E. E. Machulskaya, M. V. Glagolev, and V. N. Lykosov, 2011: Modeling of methane emissions from lakes in the permafrost zone. *Izvestiya, Atmospheric and Ocean Physics*, **47,** 1-14.

Stepanenko, V. M., S. Goyette, A. Martynov, M. Perroud, X. Fang, and D. Mironov, 2010: First steps of a Lake Model Intercomparison Project: LakeMIP. *Boreal Environment Research*, **15,** 191-202.

Tranvik, L. J., and Coauthors, 2009: Lakes and reservoirs as regulators of carbon cycling and climate. *Limnology and Oceanography*, **54,** 2298-2314.

Vassiljev, J., S. P. Harrison, S. Hostetler, and P. J. Bartlein, 1994: Simulation of Long-Term Thermal-Characteristics of 3 Estonian Lakes. *Journal of Hydrology*, **163,** 107-123.

Vavrus, S. J., R. H. Wynne, and J. A. Foley, 1996: Measuring the sensitivity of southern Wisconsin lake ice to climate variations and lake depth using a numerical model. *Limnology and Oceanography*, **41,** 822-831.

Verburg, P., and R. E. Hecky, 2009: The physics of the warming of Lake Tanganyika by climate change. *Limnology and Oceanography*, **54,** 2418-2430.

Vesala, T., and Coauthors, 2006: Eddy covariance measurements of carbon exchange and latent and sensible heat fluxes over a boreal lake for a full open-water period. *Journal of Geophysical Research-Atmospheres*, -.

Vickers, D., and L. Mahrt, 1997: Fetch limited drag coefficients. *Boundary-Layer Meteorology*, **85,** 53-79.

Vincent, A. C., D. R. Mueller, and W. F. Vincent, 2008: Simulated heat storage in a perennially ice-covered high Arctic lake: Sensitivity to climate change. *J. Geophys. Res.-Oceans*, **113**.

Walter, K. M., L. C. Smith, and F. S. Chapin, 2007: Methane bubbling from northern lakes: present and future contributions to the global methane budget. *Philosophical Transactions of the Royal Society a-Mathematical Physical and Engineering Sciences*, **365,** 1657-1676.

Walter, K. M., S. A. Zimov, J. P. Chanton, D. Verbyla, and F. S. Chapin, 2006: Methane bubbling from Siberian thaw lakes as a positive feedback to climate warming. *Nature*, **443,** 71-75.

Wetzel, R., and G. E. Likens, 1991: *Limnological analyses.* Springer-Verlag.

Yeates, P. S., and J. Imberger, 2003: Pseudo two-dimensional simulations of internal and boundary fluxes in stratified lakes and reservoirs. *International Journal of River Basin Management*, **1,** 297 - 319.

Zeng, X., M. Shaikh, Y. Dai, R. Dickinson, and R. Myneni, 2002: Coupling of the common land model to the NCAR community climate model. *J. Clim.*, **15,** 1832-1854.

Zhang, T., and M. O. Jeffries, 2000: Modeling interdecadal variations of lake-ice thickness and sensitivity to climatic change in northernmost Alaska. *Annals of Glaciology, Vol 31, 2000,* K. Steffen, Ed., 339-347.

Zhang, Y. Z., J. Pulliainen, S. Koponen, and M. Hallikainen, 2003: Empirical algorithms for Secchi disk depth using optical and microwave remote sensing data from the Gulf of Finland and the Archipelago Sea. *Boreal Environment Research*, **8,** 251-261.

Zilitinkevich, S. S., 1972: *The dynamics of the atmospheric boundary layer*. National Lending Library for Science and Technology.

Zilitinkevich, S. S., A. A. Grachev, and C. W. Fairall, 2001: Scaling reasoning and field data on the sea surface roughness lengths for scalars. *Journal of the Atmospheric Sciences*, **58,** 320-325.

Figures for Review

Z.M. Subin and W.J. Riley
Lawrence Berkeley National Laboratory

D. Mironov
German Weather Service

December, 2011

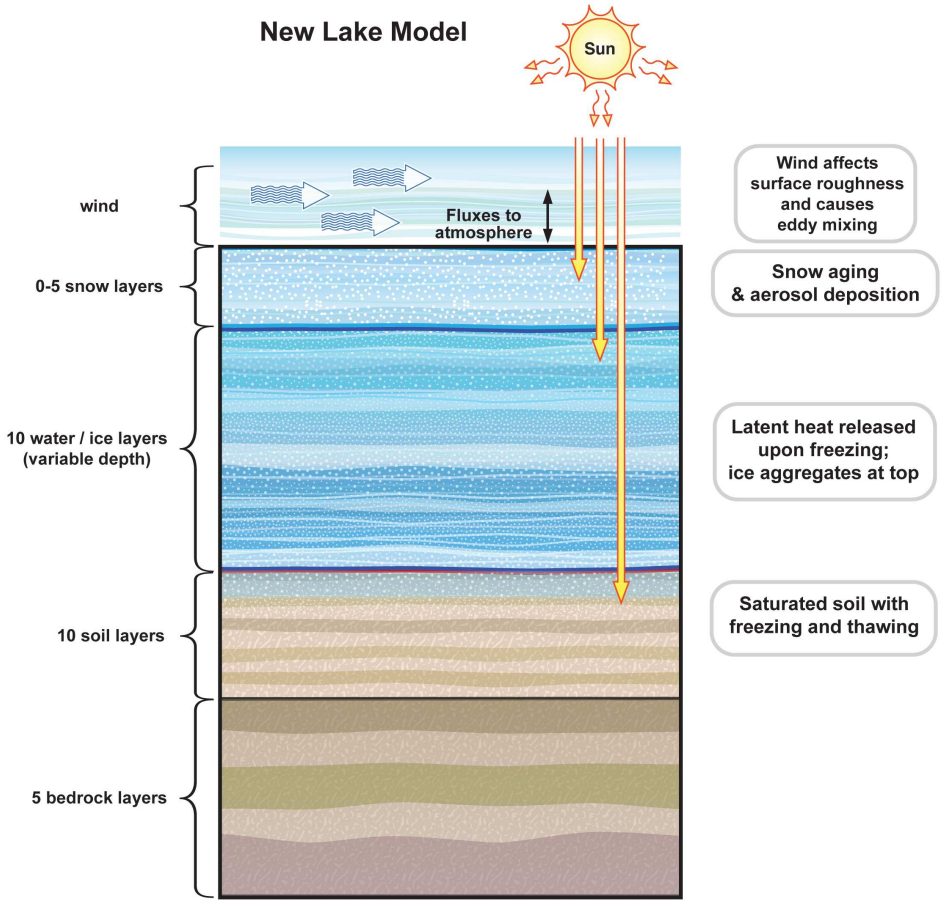

Figure 1: Lake Model Schematic

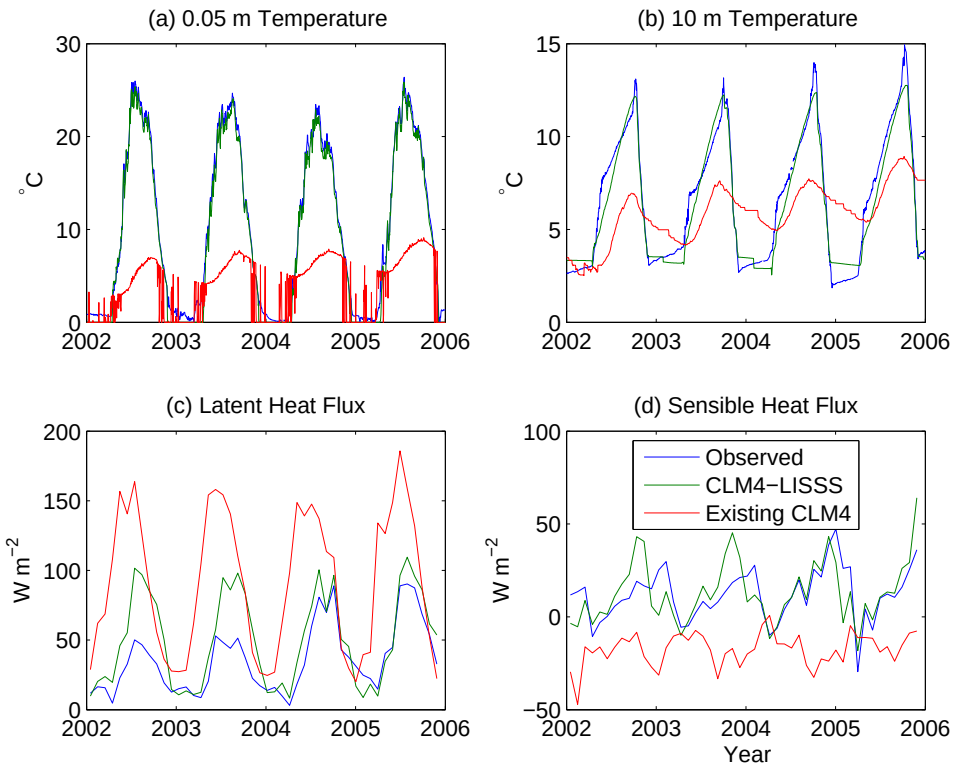

Figure 2: Daily mean Sparkling Lake water temperatures and 30-day mean surface energy fluxes, 2002-2005, observed, simulated by CLM4-LISSS, and simulated by the existing CLM4 lake model: (a) 0.05 m water temperature (below-freezing temperatures are not shown, as surface observations are typically flawed during these periods); (b) water temperature at 10 m depth; (c) latent heat flux; and (d) sensible heat flux.

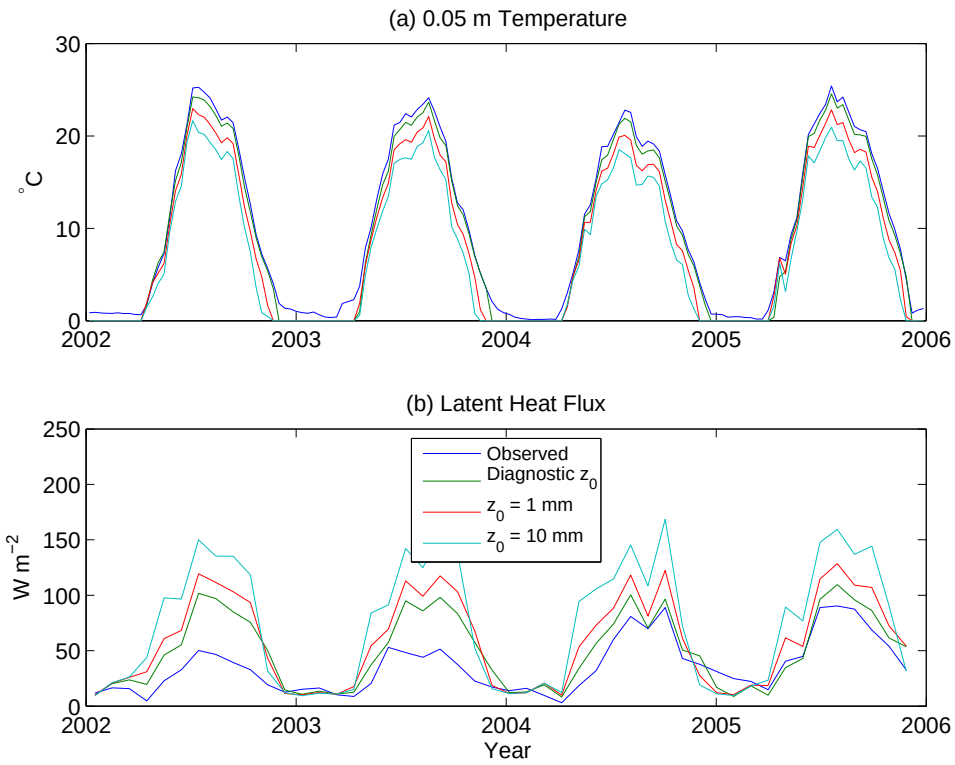

Figure 3: Ten-day mean Sparkling Lake (a) 0.05 m temperature and (b) latent heat flux, 2002-2005, observed and simulated by CLM4-LISSS with diagnostic roughness lengths, fixed 1 mm roughness lengths, and fixed 10 mm roughness lengths. Near-surface below-freezing temperatures are not shown, as surface observations are typically flawed during these periods.

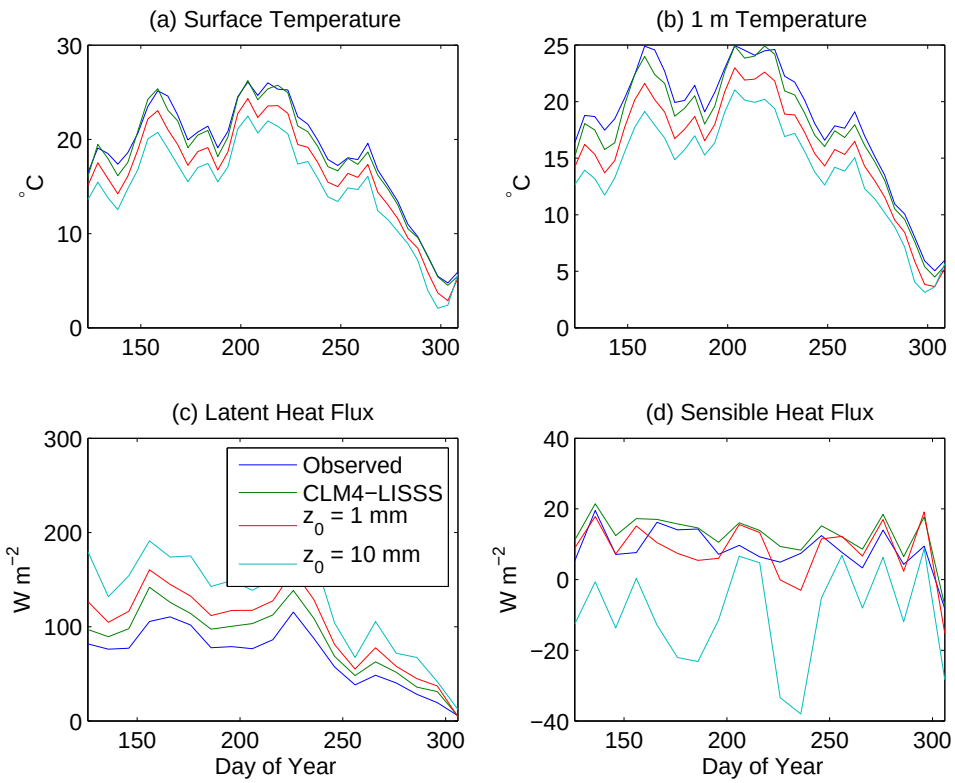

Figure 4: Five-day mean Kossenblatter water temperatures and surface energy fluxes, May - November, 2003, observed and simulated by CLM4-LISSS with diagnostic roughness lengths, fixed 1 mm roughness lengths, and fixed 10 mm roughness lengths: (a) surface temperature; (b) temperature at 1 m depth; (c) latent heat flux; and (d) sensible heat flux.

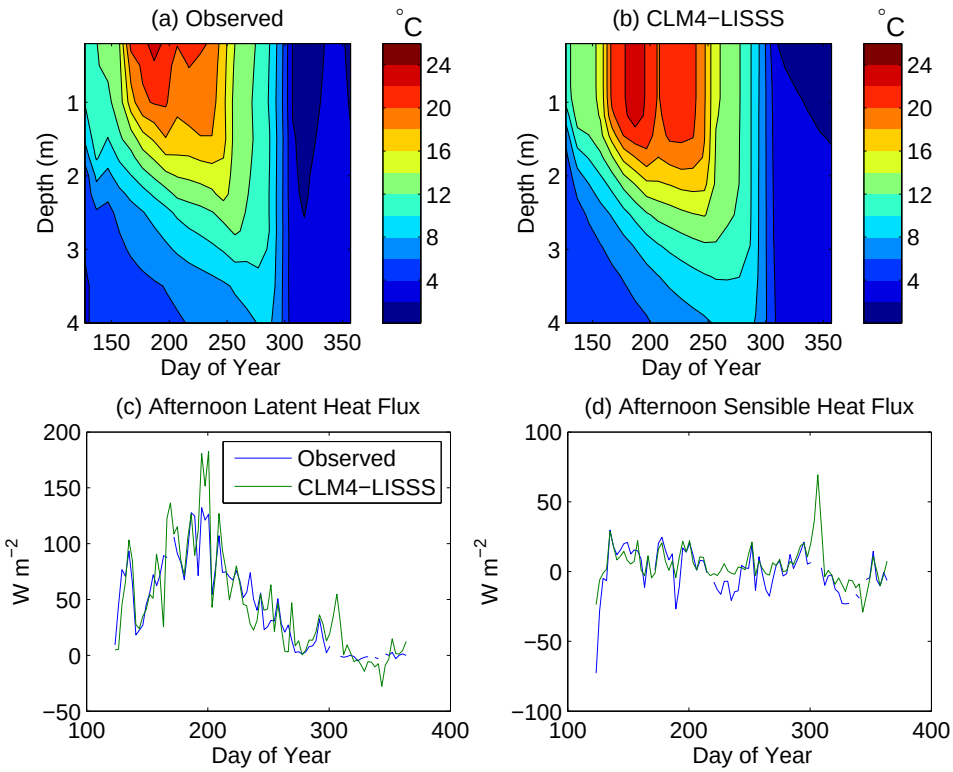

Figure 5: Lake Valkea-Kotinen, May - December, 2006. Ten-day mean water temperatures: (a) observed (Nordbo et al. 2011); and (b) simulated by CLM4-LISSS. Three-day mean (over available data for the sporadic observations) 12-6 PM surface energy fluxes: (c) latent heat flux; and (d) sensible heat flux.

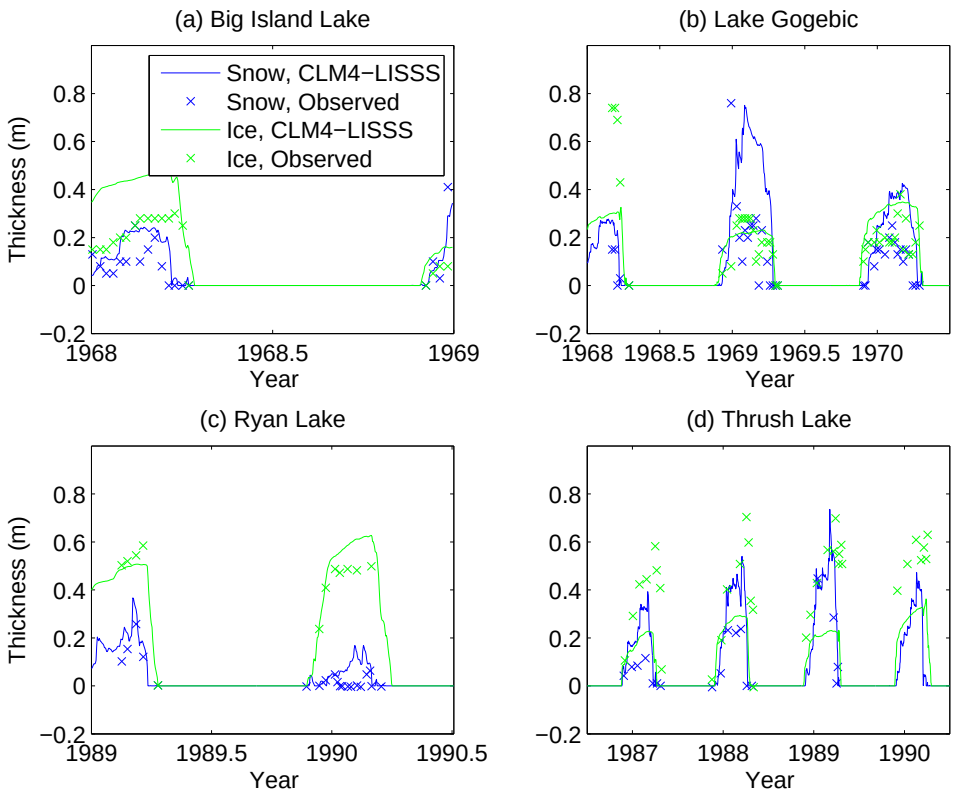

Figure 6: Snow thickness and ice thickness, simulated by CLM4-LISSS and observed, for (a) Big Island Lake; (b) Gogebic Lake; (c) Ryan Lake (Gu and Stefan 1993); and (d) Thrush Lake (Fang and Stefan 1996).

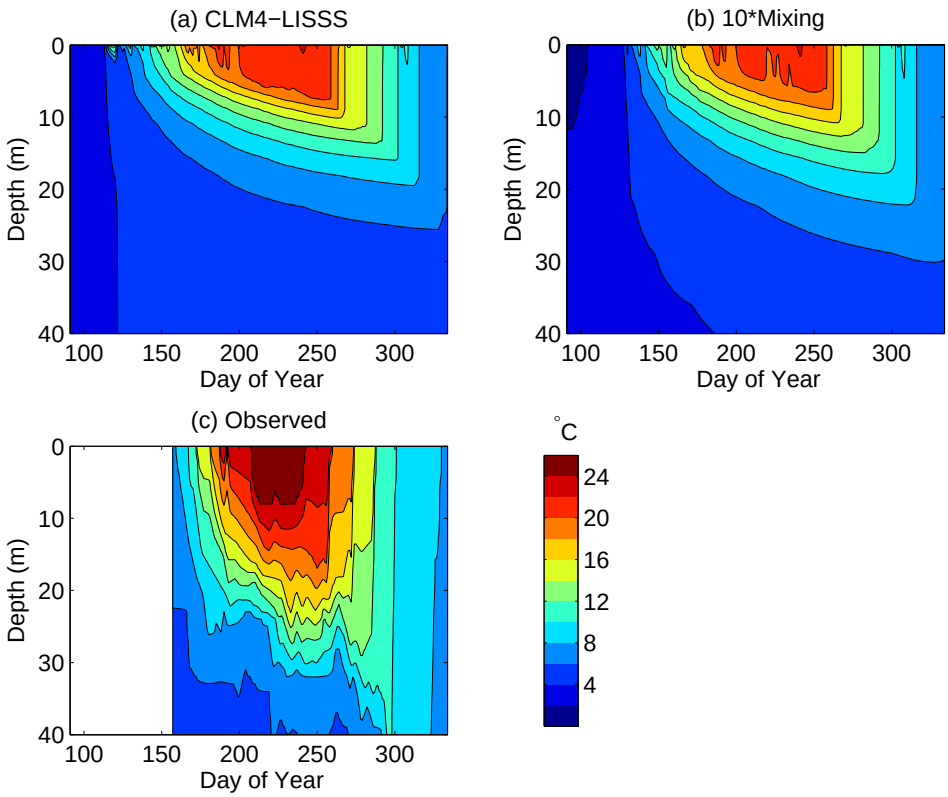

Figure 7: Daily mean Lake Michigan water temperatures for 1990: (a) CLM4-LISSS; (b) eddy diffusivity increased by 10; and (c) observed (McCormick and Pazdalski 1993).

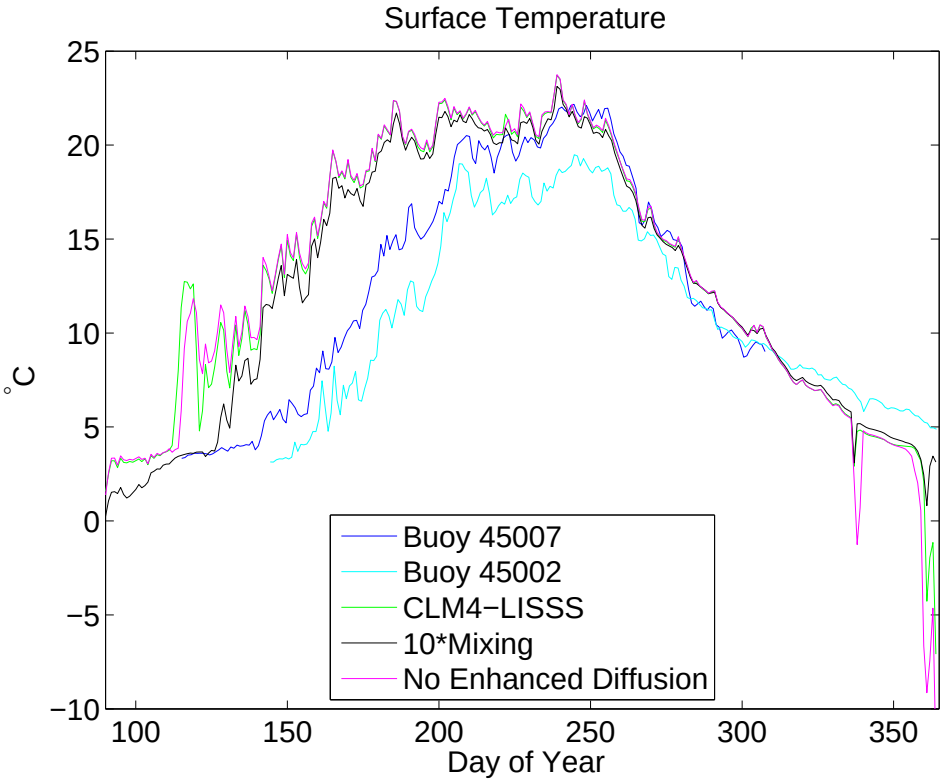

Figure 8: Daily mean Lake Michigan surface temperatures for 1990: National Data Buoy Center Station 45007 observations, National Data Buoy Center Station 45002 observations, and simulated by CLM4-LISSS, CLM4-LISSS with eddy diffusivity increased by 10, and CLM4-LISSS with no enhanced diffusion.

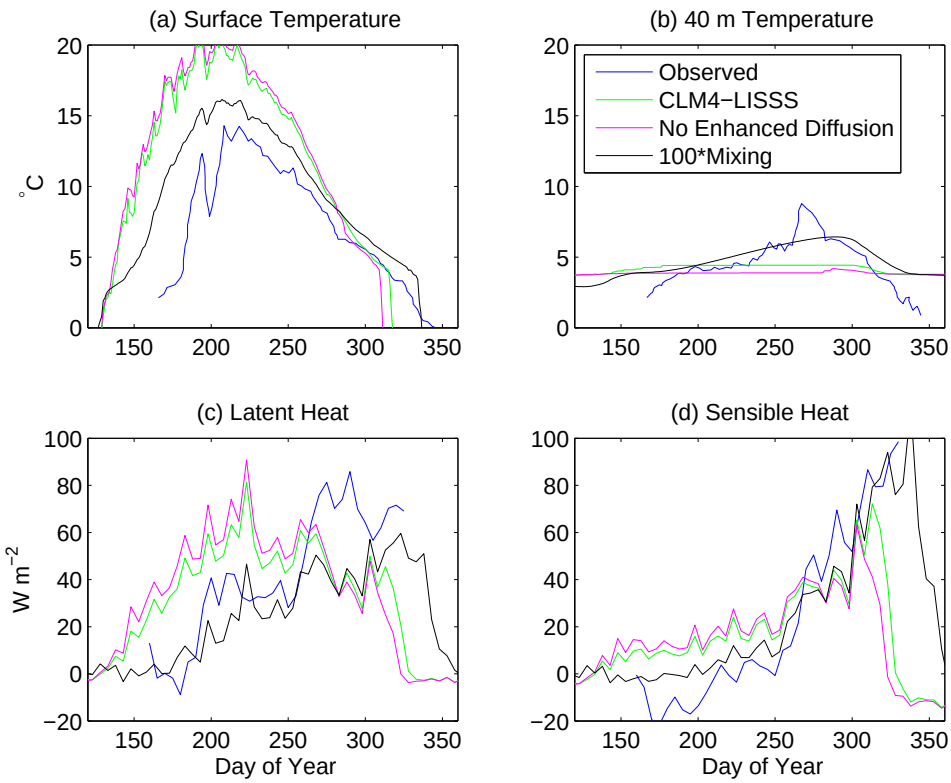

Figure 9: Daily-averaged Great Slave Lake water temperatures and surface fluxes from 1997-2003 excluding 2001, observed (Rouse et al. 2008) and simulated by CLM4-LISSS, CLM4-LISSS with no enhanced diffusion, and CLM4-LISSS with eddy diffusivity increased by 100: (a) surface temperature; (b) temperature at 40 m depth; (c) latent heat; and (d) sensible heat.

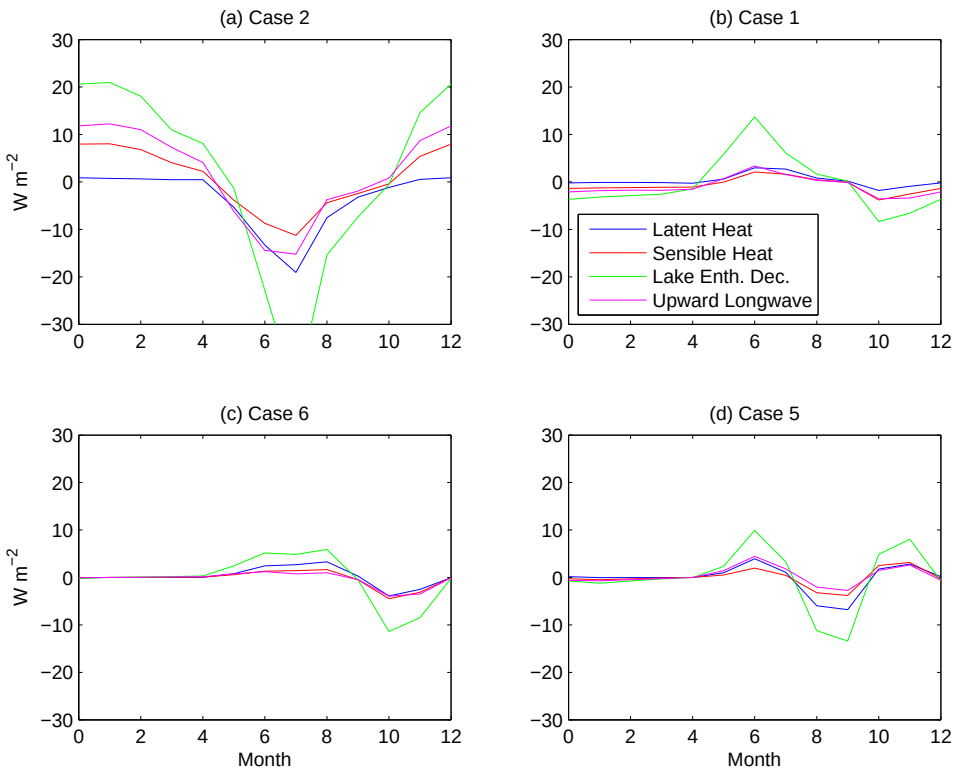

Figure 10: Monthly average surface flux anomalies for North Eurasian (60 - 90 °N, 0 - 175 °E) lakes, latent heat, sensible heat, rate of lake enthalpy decrease, and upward longwave: (a) Case 2, no snow insulation; (b) Case 1, no heat of fusion for phase change; (c) Case 6, lake depth = 5 m; and (d) Case 5, lake depth = 50 m.

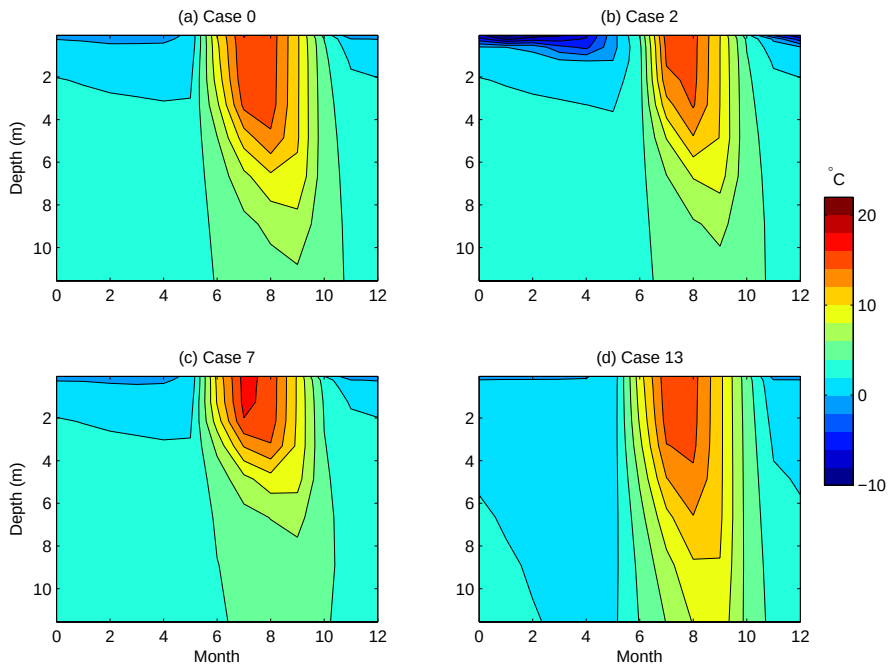

Figure 11: Monthly average water temperatures for the gridcell co-located with Finnish lake Inari: (a) Case 0, baseline; (b) Case 2, no snow insulation; (c) Case 7, extinction coefficient = 1.0 m^{-1}; and (d) Case 13, eddy diffusivity increased by 10.

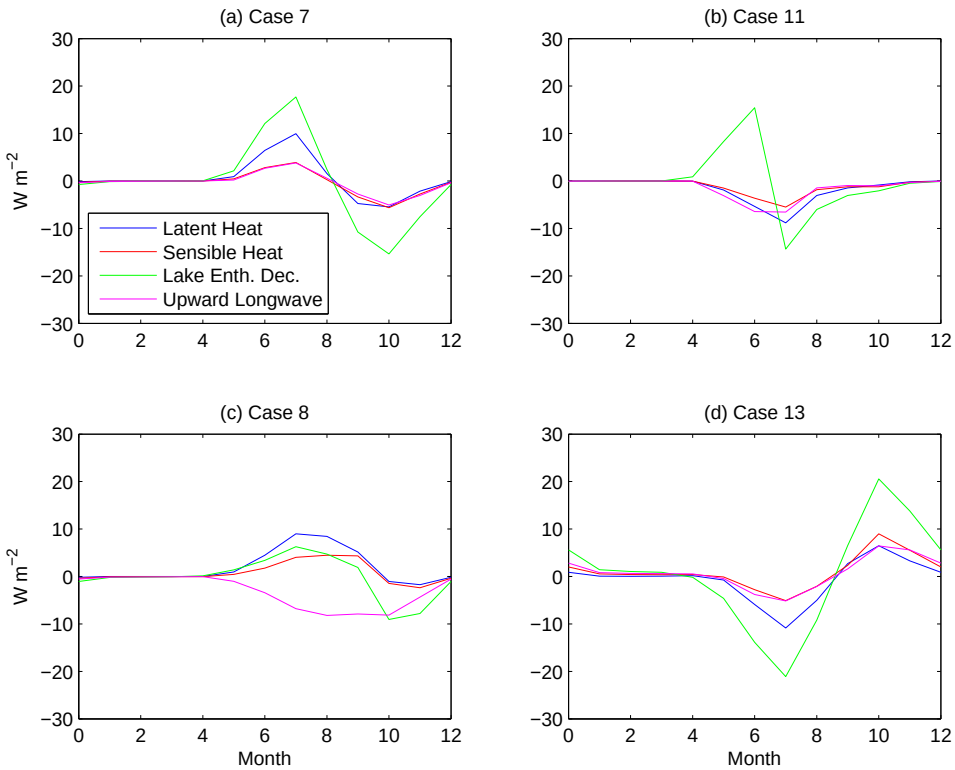

Figure 12: Monthly average surface flux anomalies for North Eurasian (60 - 90 °N, 0 - 175 °E) lakes, latent heat, sensible heat, rate of lake enthalpy decrease, and upward longwave: (a) Case 7, extinction coefficient = 1.0 m^{-1}; (b) Case 11, no albedo correction for melting lakes; (c) Case 8, roughness lengths = 1 mm; and (d) Case 13, eddy diffusivity increased by 10.